How do Dachsous and Fat polarise cells in the larval abdomen of *Drosophila*?

Stefano Pietra[1], KangBo Ng[1,2], Peter A. Lawrence[1], José Casal[1]

[1] Department of Zoology, University of Cambridge, Downing Street, Cambridge CB2 3EJ, United Kingdom
[2] Current Address: The Francis Crick Institute, 1 Midland Road, London NW1 1AT, United Kingdom

ABSTRACT

We investigate the mechanisms of planar cell polarity (PCP) in the larval epidermis of *Drosophila*. Measurements of the amount of Dachsous across the segment find a peak located near the rear of the anterior compartment. Localisation of Dachs and orientation of ectopic denticles reveal the polarity of every cell in the segment. We discuss how well these findings evidence a zigzag gradient model of Dachsous activity. Several groups have proposed that Dachsous and Fat fix the direction of PCP via oriented microtubules that transport PCP proteins to one side of the cell. We test this proposition in the larval cells and find that most microtubules grow perpendicularly to the axis of PCP. We find no significant bias in the polarity of those microtubules aligned close to that axis. We also reexamine published data from the pupal abdomen and fail to find evidence supporting the hypothesis that microtubular orientation draws the arrow of PCP.

INTRODUCTION

As cells construct embryos and organs they need access to vectorial information that informs them, for example, which way to migrate, divide, extend axons or how to orient protrusions. In *Drosophila* there are (at least) two conserved genetic systems

that generate vectorial information, and here we are concerned with only one of those, the Dachsous/Fat system. Dachsous (Ds) and Fat (Ft) are large atypical cadherin molecules that form heterodimeric bridges from cell to cell that help build planar cell polarity (PCP) in one cell and also convey polarity between cells (***Ma et al., 2003; Matakatsu and Blair, 2004; Casal et al., 2006; Lawrence and Casal, 2018***). The activity of Ft is increased and Ds is reduced when they are phosphorylated by a third molecule, Four-jointed (Fj), a Golgi-based kinase (***Ishikawa et al., 2008; Brittle et al., 2010; Simon et al., 2010***). The distribution of Ds, Ft and Fj and the interaction between these molecules together determine what we describe as "Ds activity", by which we mean the propensity of Ds on one cell to bind to Ft in the neighbouring cell. Experiments suggest that, using the disposition and orientation of Ds-Ft bridges, each cell compares the Ds activity of its two neighbours and points its denticles towards the neighbour with the higher Ds activity. In this way, the local slopes in a landscape of Ds activity determine polarities of all the cells (***Casal et al., 2002;*** see ***Lawrence and Casal, 2018*** for more explanation).

A model: the ventral epidermis of the *Drosophila* larva

Each segment of the larva is divided by cell lineage into an anterior (A) and a posterior (P) compartment. In the ventral epidermis, a limited region of the segment makes rows of thorny denticles that are polarised in an almost invariant pattern, while the larger part of each segment makes no denticles and therefore its polarity is not known (***Figure 1– figure supplement 1***). The Ds/Ft system is alone effective in building PCP in the denticulate epidermis, there being little or no contribution from the "core" or Stan/Fz system (***Casal et al., 2006; Repiso et al., 2010; Donoughe and DiNardo, 2011***). In the adult abdomen the A and P compartments are thought to be approximately coextensive with opposing gradients of Ds activity that drive opposing polarities (***Casal et al., 2002***).

A molecular model has been built of how the Ds/Ft system generates polarity information in the ventral larval epidermis. In the latest form of this model the polarities of all the denticles are readouts of a zigzag landscape of "Ds activity" ***(Rovira et al., 2015; Saavedra et al., 2016)***. Here we present four molecular and genetic tests of the model, which we extend to the uncharted region of the segment.

The **first test** is to drastically change the Ds distribution *in vivo* by experiment and then study individual cells and parts of cells in these larvae that we refer to as "polarity modified". The results support the model.

The **second test** is to measure directly the amounts of Ds protein localised to abutting pairs of membranes in the wildtype. We validate the method used by measuring Ds protein distribution in "polarity modified" larvae. In the wildtype there is a peak of Ds amounts near the back of the A compartment, consistent with the model.

The **third test** is to use Dachs (D), a molecule downstream of Ds and Ft that localises asymmetrically, ie on one side of the cell. The distribution of tagged D (***Mao et al., 2006***) in individual cells indicates their molecular polarities (***Mao et al., 2006; Brittle et al., 2010; Ambegaonkar et al., 2012; Bosveld et al., 2012; Ambegaonkar and Irvine, 2015***). We find that undenticulated cells of the P compartment accumulate D on their posterior membrane while undenticulated cells of the A compartment (apart from one row of cells at the extreme rear of that compartment) accumulate D on their anterior membrane.

The **fourth test** is an alternative and independent assessment of cell polarity in undenticulated cells. We induce oriented denticles in normally undenticulated cells by making small clones that overexpress a particular gene *(*ovo ***Delon et al., 2003)***. The results are exactly consistent with our observations of D localisation.

The **fifth test** is concerned with microtubules. Given that the overall model is substantiated by the previous four tests we now ask: how is this polarity information, generated by the Ds/Ft system, translated into cell and denticle polarity? Harumoto et al reported that in one particular region of the pupal wing of *Drosophila* the majority of microtubules are aligned near-parallel with the axis and direction of PCP (the direction of PCP is defined by the orientation of hairs) and, when growing, they show a small but statistically significant "bias" in polarity (***Harumoto et al., 2010***). By bias we mean a net difference in the number of microtubules growing within a particular angle interval —say 135 to 225 degrees— and the number of microtubules growing 180 degrees away —315 to 45 degrees— for instance we might see more microtubules growing distally than proximally. Harumoto et al therefore proposed that, in general,

the Ds/Ft system controls the polarity of microtubules that subsequently orient cells (***Harumoto et al., 2010***). Tests of this hypothesis in the adult abdomen have given mixed results (***Matis et al., 2014; Olofsson et al., 2014; Sharp and Axelrod, 2016***). Newer results from both wing and the abdomen are conflicting; regions of both appear to be polarised independently of the microtubules (***Sharp and Axelrod, 2016***). In the hope of clarifying this confusing situation we therefore study microtubule orientation *in vivo* in the larva. The larva has advantages over imaginal discs or the adult abdomen: individually identifiable cells have a defined polarity and larval cells are much larger than the adult cells. Several analyses of our own results on the larval abdomen and of raw data kindly provided by Axelrod from the pupal abdomen (***Olofsson et al., 2014; Sharp and Axelrod, 2016***) do not support the hypothesis that PCP is oriented by microtubules.

RESULTS

Building a model of Ds/Ft in the larval PCP

We put forward a general hypothesis that, in the segment, opposing gradients of Ds activity are translated into PCP (***Casal et al., 2002; Lawrence and Casal, 2018***). But that simple model could not encompass the more complex reality of the larva and its denticle rows. We discovered, in the larva, 3 stripes of specialised cells per segment and two of these (T1 and T2, see ***Figure 1***) express the modifier *fj* which reduces Ds activity (***Saavedra et al., 2016***). The local slopes of the resulting zigzag landscape of Ds activity (***Figure 1B***) would then be read out as denticle orientation, but how? We proposed that, within a cell, there is a local comparison between membranes that face each other, so that denticles lying between two membranes always point towards that membrane that presents the lower Ds activity (implying that, in the adjacent cell, there is more Ds activity;***(Casal et al., 2002; Lawrence and Casal, 2018)***. We suggested that conduits could span across the cell to mediate the comparison. No such conduits have been identified but they could be microtubules or other organelles (***Burute and Kapitein, 2019***).

Test 1 Testing the model in the wildtype and polarity modified larvae

(i) Polarity of typical cells

The model posits that the polarity of each cell, or part of cell, depends on a comparison of mutually facing membranes. Thus, in the wildtype, a low activity of Ds due in part to high expression of *fj* in T1 and T2, orients the denticles in the adjacent rows (1, 2 and 4, 5) to point outwards from T1 and T2 (***Rovira et al., 2015; Saavedra et al., 2016***). We have compared the polarity of the predenticles in wildtype (***Figure 1***; ***Rovira et al., 2015; Saavedra et al., 2016***) and in "polarity modified" larvae (***Figure 2***). In the polarity modified larvae, we engineer increased expression of *ds* in T1 and T2 cells; this changes the landscape of Ds activity, making peaks (instead of troughs, as in the wildtype) in T1 and T2. Consequently, the polarities of rows of cells 1, 2, 4 and 5, that abut T1 and T2, now point inwards, that is reversed from the wildtype (***Figure 2A-C***). The other rows, 0, 3 and 6 could also be affected because polarity can be propagated beyond the neighbouring cells (***Repiso et al., 2010; Donoughe and DiNardo, 2011; Saavedra et al., 2016***). Our present findings confirm previous ones (***Saavedra et al., 2016***).

(ii) Atypical cells

The numbered cell rows are often irregular and some cells are "atypical", meaning that one face of a cell abuts two different neighbours, each with a different level of Ds activity: consequently, individual cells can display two different predenticle and denticle polarities, depending on the Ds activities of the facing neighbours (***Rovira et al., 2015***). We now compare the predenticles of atypical cells in wildtype and polarity modified larvae in order to test the validity of the model in both situations. In the wildtype, one posterior part of cell ***a*** in row 4 may contact a T2 neighbour with a lower Ds activity than row 3 (the associated predenticles in this region of cell ***a*** point anteriorly) and a separate part of cell ***a*** may contact a row 4 neighbour with a higher Ds activity than row 3 (the associated predenticles in this other region of cell ***a*** mostly point posteriorly ***Rovira et al., 2015***). However, in the polarity modified larvae, the predenticles of nearly all cells of row 4 (typical and atypical cells) point posteriorly—this is as expected from the model because ***both*** types of posterior and abutting neighbours (T2 and row 4) now have higher levels of Ds activity than the anterior

148 neighbour, a row 3 cell (***Figure 2D-F*** and ***Table 1***). However for these larvae, some
149 single atypical cells of row 2 have two anterior neighbours, —cells of T1 and row 2—
150 that are higher and lower in Ds activity than the posterior neighbour of the atypical
151 cell, respectively. Consequently, the model predicts that their associated predenticles
152 should point forwards in that part of the cell that abuts T1 and backwards in that part
153 of the same cell abutting row 2, and they do (***Figure2 G-I*** and ***Table 1***). There are
154 some quantitative differences between the current data and the wildtypes we scored
155 earlier ***(Rovira et al., 2015, see legend to Table 1)***. Nevertheless, these results confirm
156 and strengthen the model.

157 Test 2 Direct assessment of Ds distribution in both wildtype and polarity 158 modified larvae

159 We measure the native Ds distribution using a tagged Ds molecule expressed as in the
160 wildtype. Ds accumulates as puncta in the membrane ***(Figure 3 Ma et al., 2003;***
161 ***Brittle et al., 2012)*** and, presumably, the puncta contain or consist of Ds-Ft
162 heterodimers (***Hale et al., 2015***).

163 We previously inferred but did not show directly a supracellular gradient in Ds
164 activity rising from front to back of the A compartment and falling into P (***Casal et***
165 ***al., 2002***). We therefore quantified and compared the amount of Ds localised at cell
166 junctions in all rows of the segment in the larval ventral epidermis. These
167 measurements do not evidence an overall gradient. However, there is a statistically
168 significant peak in both junctions 9/T3 and T3/10; these are located near the rear of
169 the A compartment. (***Figure 4***). We tested the quantitation technique in polarity
170 modified larvae and find that the distribution of Ds is altered from the wildtype as
171 expected (***Figure 4–figure supplement 1***). This successful test of the method confirms
172 the existence of a peak of Ds amount near the back of the A compartment in the
173 wildtype (***Figure 4***).

174 Test 3 The location of D

175 The myosin-related molecule D is a marker of polarity and localised by the Ds/Ft
176 system (***Mao et al., 2006; Rogulja et al., 2008; Bosveld et al., 2012; Brittle et al.,***
177 ***2012; Lawrence and Casal, 2018***). It is usually asymmetrically distributed on a

178 polarised cell and is thought to co-localise with the face of the cell associated with the
179 most Ds (***Mao et al., 2006; Rogulja et al., 2008; Brittle et al., 2012***). We map D to the
180 membranes of individual cells in the larval epidermis by making small clones of cells
181 that express tagged D; this allows the distribution of D on a particular cell to be
182 assessed so long as the neighbour(s) does not contain any tagged D.

183 We examine the distribution of D in wildtype larvae in order to test the PCP
184 model and to reveal the molecular polarity of cells that lack denticles (***Figure 5 and 6***).
185 In the P compartment, all the denticulate and undenticulate cells show a consistent
186 molecular polarity, D being localised posteriorly in the cell. Most cells of the A
187 compartment have the opposite polarity, with D located anteriorly. In both
188 compartments, the location of D in the denticulate cells correlates in all cases with the
189 denticle polarity, and this includes the cells of rows 0, 1 and 4 whose denticles point
190 forward. The muscle attachment cells, T1,T2 and T3 can express D but it is mostly
191 cytoplasmic in location. The cells flanking T1 and T2 accumulate D at the membrane
192 abutting the tendon cells. Unlike all the other rows, cells of row 11 show some
193 variation in the localisation of D: about 45% localise it at the cell membrane in the
194 back, as do cells in the P compartment, in 35% its at the membrane but not
195 asymmetrically localised and, in the remaining cells, D is either at the front or found
196 only in the cytoplasm (***Figure 6***). This means that the line where polarity changes
197 from the A-mode to the P-mode is not at the A/P border (***Casal et al., 2002***) but in
198 front of it; suggesting that the second cell row anterior to the A/P cellular interface
199 (row 10) contains the peak level of Ds activity. From that row effects on polarity
200 spread forwards into the A compartment and backwards into row 11 and the P
201 compartment. (see model in ***Figure 9***).

202 The localisation of D is not always continuous along the rear (or the front)
203 membrane of a cell. When the plasma membrane of one side of an atypical cell **a** abuts
204 two separate cells, and our model implies that these two cells have different levels of
205 Ds activity, then the D from cell **a** is localised at the interface with just one of those
206 cells, on that part of the membrane that has most Ds activity (cells 10 and 11 in ***Figure***
207 ***5C***, and ***Figure 5–figure supplement 1A***, see legend). This suggests that different parts
208 of a single cell's membrane can compete for D.

209 What is the distribution of D in larvae that lack the Ds or Ft protein (*ds*⁻ or *ft*⁻?
210 To our surprise, although D distribution was variable in location and was more diffuse
211 than the wildtype, D can be asymmetrically localised at the membrane, but in a
212 disorganised way. We found no consistent difference between *ds*⁻ and *ft*⁻ larvae
213 (***Figure 5–figure supplement 1B, C***). Thus it appears that some asymmetric
214 localisation of D can occur independently of Ds-Ft heterodimers (which should be
215 missing in *ds*⁻ and *ft*⁻ larvae).

216 Test 4. *ovo*-expressing clones reveal otherwise unseen polarity.

217 Small clones that overexpress *ovo* in naked areas often produce denticles in embryos
218 (***Delon et al., 2003; Walters et al., 2006***). We made marked clones in larvae and these
219 also generally made denticles. The denticles showed a consistent orientation, pointing
220 forwards in P and backwards in most of A, exactly mirroring the polarity pattern as
221 identified by D localisation (***Figure 7,*** compare with ***Figure 6***). Thus, cell of row 11 at
222 the back of the A compartment mostly made denticles that pointed forwards (***Figure***
223 ***7***) as is characteristic of cells belonging to the P compartment. Just as signalled by the
224 localisation of D, in a minority of row 11 cells, polarity was ambiguous with denticles
225 pointing in various directions (***Figure 7–figure supplement 1***). The denticles
226 belonging to the cell row 10 in front of row 11 always pointed backwards and denticles
227 of the row behind row 11 (row -2 of the P compartment) always pointed forwards.

228 Test 5. Does the orientation of growing microtubules correlate with PCP?

229 We study the orientation of growing microtubules (using EB1 comets ***Schuyler and***
230 ***Pellman, 2001; Akhmanova and Steinmetz, 2008***) in the large epidermal cells of the
231 ventral larva. Our main data is collected from identified A cells of rows 7-8 (direction
232 of PCP is posterior) and identified P cells of rows -2 and -1 (direction of PCP is
233 anterior; ***Figure 6***); the classification of the A and P cells as having opposite polarities
234 is based on studies of the larval ventral abdomen described above and confirmed by
235 Tests 3 and 4, above. To assess the orientation of growing microtubules, we took 10
236 larvae, made films and studied one A and one P cell from each (***Figure 8–movie***
237 ***supplement 1,2***). The growing microtubules were then recorded vis-à-vis the axis of
238 the larva by one person (SP) who was blinded to the identity of each of the 20 cells he

239 was scoring. The orientations of about 4000 EB1 comets are shown and analysed in
240 ***Figure 8***.

241 In the wing, the predominant alignment of the microtubules is close to the axis
242 of PCP (***Harumoto et al., 2010; Gomez et al., 2016***). By contrast, in the larval
243 epidermal cells, in both A and P compartments, the majority of the microtubules are
244 aligned perpendicular to the anteroposterior axis, the axis of PCP (***Figure 8A,B***). To
245 analyse our data and following the approach in the wing, the comets of the larvae are
246 sorted into four 90 degree quadrants centred on the anteroposterior and mediolateral
247 axes and their frequencies plotted. The quadrants are described as "anterior",
248 "posterior", "medial" and "lateral" (***Figure 8C,D***). The axis of PCP lies in the
249 anteroposterior axis, but, in A compartment cells, 66% of the total angles of growth
250 fall within the medial and lateral sectors, while in the P compartment the comparable
251 figure is 71%. Clearly there is no overall correlation between microtubular orientation
252 and PCP and this belies the hypothesis that microtubular orientation is causal for
253 PCP.

254 However, we could look for a limited correlation between the orientation of
255 growing microtubules and the direction of PCP. For example, considering only the
256 minority of microtubules within the anterior and posterior sectors, we find small
257 differences in polarity but they lack statistical significance (***Figure 8C,D***). In A cells
258 the proportion of all microtubules that grow anteriorly is 15.8% with a 95% CI of [13.5
259 to 18.2] and the proportion that grow posteriorly is 18.3% [15.9 to 20.6]. In P cells it is
260 the reverse; 16.7% grow anteriorly [14.4 to 19.1] and the proportion that grow
261 posteriorly 12.7% [10.3 to 15.0]. There was a comparable and also non significant bias
262 in the medial and lateral quadrants: in A cells a larger proportion of all microtubules
263 grow medially 34.4%[32.0 to 36.8] and 31.5% [29.1 to 33.8] laterally while the reverse
264 bias occurs in P cells where more microtubules grow laterally 36.9% [34.5 to 39.2]
265 than medially 33.7% [31.4 to 36.1] (***Figure 8C,D***).

266 How uniform are the individual cells? To answer we group all the growing
267 microtubules according to which cell (and larva) they come from and according to
268 which of four 90 degree quadrants they fall into (***Figure 8E***). Remarkably, in all sets,
269 individual cells differ wildly from each other. Comparing the anterior versus posterior

and medial versus lateral quadrants we find no strong evidence for a bias in the directions in which the microtubules grow —apart from the main finding that most of the microtubules grow more or less perpendicular to the axis of PCP.

Could there be a special subset of oriented microtubules perhaps aligned close to the anteroposterior axis, the axis of PCP, that might show a polarity bias that related to some function in planar polarity? There is no independent evidence favouring such a perspective. Nevertheless, to check we scan through the entire circumference in 22.5 degree sectors, measuring the amount of bias in the microtubules that fall within opposite pairs of sectors. There is no increase in bias in the sectors that included the axis of PCP in either the A or the P compartments, nor in nearby sectors. However, there is a local peak of bias within the A compartment: there is a significant bias in the number of growing microtubules within one pair of 22.5 degree sectors that is far away from the axis of PCP. Within the P compartment a similar peak of bias is centred near the mediolateral axis within two facing 22.5 degree sectors (***Figure 8–figure supplement 1***) But note that these biases represent only 2-3% of the total population of microtubules. Thus, although we found some irregularities in the circular distribution of growing microtubules, we find no correlation with the axis of PCP.

Axelrod's group kindly made their raw data from the pupal abdomen available to us and we treat them exactly as our larval data. To analyse, Axelrod's group grouped the pupal comets into two unequal sets (170 and 10 degrees***, Olofsson et al., 2014; Sharp and Axelrod, 2016***). But to conform with how data on the wing has been presented (***Harumoto et al., 2010; Olofsson et al., 2014; Sharp and Axelrod, 2016***), and to allow a comparison with our results, we subdivided their data into four 90 degree quadrants. Even more so than in the larva, the majority of the pupal microtubules are oriented orthogonally to the axis of PCP (***Figure 8–figure supplement 2A-D***): 69% of the total population of growing microtubules in the A compartment are aligned within the quadrants centred on the mediolateral axis, while in the P compartment the comparable figure is 73% (***Figure 8–figure supplement 2C,D***). This finding does not fit comfortably with a hypothesis that microtubular orientation drives PCP.

Further comparison of the Axelrod group's data on the pupa with ours on the larva show some quantitative differences. Unlike ours on the larva, their pupal data shows statistically significant biases in the orientation of comets (***Figure 8–figure supplement 2C,D***). In A cells the proportion of all microtubules that grow anteriorly is 12.7% with a 95% CI of [11.3 to 14.1]; significantly smaller than the proportion that grow posteriorly 18.1% [16.6 to 19.5]. In P cells we see a reverse bias: 15.8% [13.3 to 18.2] grow anteriorly and 11.5% [9.1 to 13.9] posteriorly. Notably, there is a comparable and also significant bias in the medial and lateral quadrants but in the same direction in both compartments. In A cells a larger proportion of all microtubules grow laterally 38.1% [36.7 to 39.6] than medially 31.1% [29.7-32.5] and a similar bias occurs in P cells where 39.8% [37.4-42.3] grow laterally and 32.9%[30.5-35.3] grow medially (***Figure 8–figure supplement 2C,D***).

We then plotted all the growing microtubules according to which pupa they came from and according to which of four 90 degree sectors they fell into (***Figure 8–figure supplement 2E***). Individual pupae differ wildly from each other. In both our results on the larva and Axelrod's results in the pupa, there is considerable inconsistency between individuals (compare ***Figure 8E*** with ***Figure 8–figure supplement 2E***). Only when all cells are taken together is there any overall and significant polarity bias in Axelrod's data.

We classified the growing microtubules in Axelrod's data into 22.5 degree sectors and looked for an orientation bias within opposite pairs of sectors. We find examples of significant bias shown by the microtubules in various sector pairs and these are mostly not near the axis of PCP. In A cells there is a statistically significant and local peak of bias ca 60-80 degrees divergent from the axis of PCP. In P cells there is a statistically significant and local peak of bias ca 35-55 degrees divergent from the axis of PCP (***Figure 8–figure supplement 1***). These observations do not fit with the conjecture that a special set of oriented microtubules, in or close to the PCP axis, might be driving planar polarity.

Dividing the data into sectors gives the impression of biases in the anteroposterior as well as in the mediolateral axes (although these are non significant in the case of the larva). But, because we suspect that subdividing the angles into

332 sectors may lead to erroneous conclusions we investigated the distributions of the
333 angles as a whole. We took the angular data of the A and P cells of the larva and pupal
334 abdomen and using a maximum likelihood model approach (***Fitak and Johnsen,***
335 ***2017***) found that the best fit in all four cases is to a bimodal distribution with two
336 peaks roughly 90 degrees divergent from the axis of PCP (***Figure 8–figure supplement***
337 ***3***). Unexpectedly, there are slight deviations of the peaks in the bimodal distributions;
338 in all four distributions one of the peaks deviates 10 degrees from the mediolateral
339 axis. Interestingly, the direction of deviation is opposite in the A cells to that in the P
340 cells; in both sets of A cells one of the peaks is tilted 10 degree toward the posterior
341 hemi-circumference, whereas in both sets of P cells one of the peaks is tilted 10
342 degrees toward the anterior hemi-circumference (***Figure 8–figure supplement 3***, see
343 legend). These opposite deviations in A and P cells may be the reason for the apparent
344 biases we observe when dividing the data into four quadrants.

345 DISCUSSION

346 A gradient model?

347 In trying to understand PCP, *Drosophila* has proved the most amenable and useful
348 experimental system. Using the *Drosophila* larva, we have built a model of how the
349 Ds/Ft system determines the pattern of polarity in the abdominal segment (***Casal et***
350 ***al., 2002; Rovira et al., 2015***). In this model the Ds/Ft system converts graded slopes
351 in the expression levels of *ds* and *fj* into local intercellular differences in the levels of
352 Ds activity, and into planar polarity without any intervention by the Stan/Fz system
353 (***Lawrence and Casal, 2018***).

354 Here we have both tested the model and extended it to those uncharted parts of
355 the larval segment that lack denticles (***Figure 9***). All the tests we have done (tests 1-4,
356 see results) are consistent with and support the model. However it is not clear whether
357 the model requires interactions between Ds, Ft and Fj to produce a multicellular
358 gradient of Ds amounts at the cell membranes, and expectations on this differ (***Hale et***
359 ***al., 2015***). We proposed that the levels of Ds activity would be graded in opposite
360 ways in the A and the P compartment and ultimately these gradients would be read

361 out as PCP in each of the cells (***Casal et al., 2002***). We imagined that gradients of Ds
362 activity would persist and this has been assumed by most (***Casal et al., 2006; Matis***
363 ***and Axelrod, 2013; Lawrence and Casal, 2018; Fulford and McNeill, 2019***) and
364 actually detected, locally, in the migrating larval epidermal cells in the pupa (***Arata et***
365 ***al., 2017***). Alternatively, once the arrow of polarity has been established in each cell, a
366 redistribution of bridges could occur and ultimately each cell would develop the same
367 numbers and disposition of bridges and, if so, no persistent multicellular gradient in
368 Ds amounts would be present (eg ***Hale et al., 2015***). Our current measurements of Ds
369 levels do not settle the matter: we did not detect a pervasive gradient of Ds, but
370 amounts were not flat either. We found a peak in Ds level located near the back of the
371 A compartment near where a Ds activity gradient was predicted to summit. However
372 a shallow Ds gradient could still exist — it might be missed because we quantify only
373 the total Ds present in abutting pairs of membranes. This shortcoming means that the
374 results can neither tell us the cellular provenance of Ds we measure, nor reveal how
375 much of it is in Ds-Ft or in Ft-Ds bridges within the apposed membranes. Thus, if any
376 cell has a higher level of Ds, this Ds will bind more Ft in the abutting cell membrane,
377 and likely tend to exclude Ds from that membrane. These effects will tend to even out
378 the amounts of Ds in joint membranes and therefore tend to disguise any gradients,
379 local peaks or troughs.

380 Could one build the segmental pattern of polarity without any initial gradient of
381 *ds* expression? If so, a localised peak in amount of Ds at the rear of the A
382 compartment (with a maximum in row 10) could affect polarity forwards into row 9
383 and propagate backwards through row 11 into the front of the P compartment. The
384 single cell troughs in Ds activity in T1 and T2 would orient the polarity of the flanking
385 cells to point away from these tendon cells. All these polarity effects would reinforce
386 each other to make a more robust pattern. However, if there were no gradient, row 3
387 would present a problem; in order to explain why it points backwards, the trough of
388 T1 in Ds activity would need to be deeper than that of T2 (see figure 4 in ***Saavedra et***
389 ***al., 2016***). The gradient and the alternative model outlined above are not mutually
390 exclusive and each can contain aspects of the truth.

391 Originally predicted to be at the A/P compartment border (***Casal et al., 2002***)
392 we conclude now that a Ds peak occurs two cells in front of that border, in row 10

(Figure 9; a similar peak two cells from the A/P border has been described in the dorsal abdomen of the pupa ***Arata et al., 2017***). This observation is supported by both D localisation and the orientation of ectopic denticles formed by *ovo*-expressing clones. There are interesting implications: the peak in Ds protein at the cell junctions is in a cell that is flanked on both sides by A compartment cells, the most posterior of which (row 11) has "P type" polarity. Why is this summit out of register with the lineage compartments? It could be that that peak is specified by a signal emanating from one compartment and crossing over to affect the next compartment. There are precedents for this (***Basler and Struhl, 1994; Diaz-Benjumea and Cohen, 1995; Doherty et al., 1996; Lawrence and Struhl, 1996; Tabata and Takei, 2004***). Also, in the abdomen of the developing adult fly, Hedgehog signal spreads from the P compartment across into the A compartment and induces different types of cuticle at different distances (***Struhl et al., 1997***).

Microtubules and PCP

We have suggested (***Rovira et al., 2015***) that intracellular conduits might be involved in a local comparison between facing membranes of a cell and shown here that this perspective successfully predicts which cells should become bipolar even in polarity modified larvae. But there is still no direct evidence for the conduits, and no knowledge of, if they do exist, what they are. One could imagine a set of microtubules, initiated on the membrane, that could align more or less with the anteroposterior axis and traverse the cell to meet the membrane opposite. Indeed, Uemura's group have proposed that wing microtubules, oriented by the Ds/Ft system, translocate vesicles carrying PCP components such as Frizzled (Fz) and Dishevelled (Dsh) to one side of a cell to polarise it. Their hypothesis began with observations on microtubule-dependent transport of tagged proteins *in vivo* in cells of the wing disc (***Shimada et al., 2006***) and was extended by the use of EB1 comets to plot microtubule polarity in the pupal wing (***Harumoto et al., 2010; Matis et al., 2014; Olofsson et al., 2014; Sharp and Axelrod, 2016***). Harumoto and colleagues studied the proximal part of the wing where they found a transient correlation, but there was no correlation in the distal wing. Also, in ds^{-} wings, distal regions show polarised microtubules without any correlation with hair polarity (***Harumoto et al., 2010***). Likewise, while some studies of

424 the abdomen reveal a local correlation between cell polarity and the orientation of
425 limited subsets of microtubules, PCP in other parts is "determined independently" of
426 the microtubules (***Sharp and Axelrod, 2016***). We have tested the hypothesis that
427 microtubular orientation drives PCP in the larval abdomen of *Drosophila* and there it
428 also meets serious difficulties. The greatest of these is that most of the microtubules
429 are aligned orthogonally to the axis of PCP (this fact is also extractable from the pupal
430 data kindly provided by Axelrod's group). Of the roughly 30% of all microtubules that
431 fall into the two quadrants centred on the axis of PCP, there is a small net excess,
432 corresponding to about 5% of the total, that could perhaps result in a net transport of
433 vesicles in the direction of PCP. But even if this were so, more than 80% of the vesicles
434 carrying cargo should arrive in the wrong part of the cell membrane.

435 Why are there apparent biases in microtubule orientation in the data? An
436 analysis of the circular distribution of comets showed, in all the sets of data (ours and
437 those of Axelrod's group), a deviation of 10 degrees in one of the peaks of the bimodal
438 distribution of the angles (***Figure 8–figure supplement 3***). This deviation, plus the
439 precise orientation of the 90 degree quadrants, may explain the apparent bias of
440 microtubular orientation seen clearly in the Axelrod data and hinted at much more
441 weakly in our data. How? Imagine a circular bimodal distribution composed of two
442 separate unimodal distributions: the tails of both probability distributions would be
443 closer and overlap more if the distance between the mean angles were reduced. In our
444 cases, the tails of the distribution whose mean angle deviate by 10 degrees will
445 decrease slightly the frequency of angles within one of the anteroposterior quadrants
446 and consequently increase the frequency in the opposite anteroposterior quadrant.
447 This deviation may have its origin in a correlation between cell shape and
448 microtubular orientation (***Picone et al., 2010; Gomez et al., 2016; Singh et al., 2018***)
449 and in different cell shapes in the A and P cells; these are more obvious at or close to
450 the A/P border (***Umetsu et al., 2014***).

451 The hypothesis of Uemura's group which proposes that microtubules transport
452 Fz to one side of the cell to polarise it meets an additional problem in the larval
453 abdomen. The normal orientations of the denticles in the larva does not require input
454 from the Stan/Fz system; indeed the Ds/Ft system appears to act alone (***Casal et al.,***
455 ***2006; Repiso et al., 2010; Donoughe and DiNardo, 2011***). But could oriented

microtubules be involved in PCP, even without any role of the Stan/Fz system? Our results from the larval abdomen say no. We cannot exclude the possibility of a small subset of stable microtubules (undetectable because they would not bind EB1), aligned with the anteroposterior axis and strongly biased in polarity, in the pupal or larval abdomens (or proximodistal axis in the wing). There is no evidence for such microtubules, but if they exist their number and bias in orientation must be strong enough to overcome the moving of vesicles on the unbiased dynamic microtubules we have studied.

To conclude, if we interrogate our data for biases in polarity within all the growing microtubules, or if we select subsets of microtubules whose orientations are related to the axis of PCP as others have done, we do not find persuasive evidence for any link between microtubular polarity and the direction of planar polarity.

MATERIALS AND METHODS

Mutations and Transgenes

Flies were reared at 25°C on standard food. The FlyBase (***Thurmond et al., 2019***) entries for the mutant alleles and transgenes used in this work are the following: *ds*: *ds*^{UA071}; *ft*: *ft*$^{G\text{-}rv}$, *ft*^{15}; *en.Gal4*: *Scer\GAL4*$^{en\text{-}e16E}$; *hh.Gal4*: *hh*^{Gal4}; *sr.Gal4*: *sr*^{md710}; *UAS.act::GFP*: *Dmel\Act5C*$^{UAS.GFP}$; *UAS.DsRed*: *Disc\RFP*$^{UAS.cKa}$; *UAS.EB1::EGFP*: Eb1$^{UAS.GFP}$; *UAS.ectoDs*: *ds*$^{ecto.UAS}$; *UAS.GFP*: *Avic\GFP*$^{S65T.UAS}$; *UAS.LifeAct::mCherry*: *Scer\ABP140*$^{UAS.mCherry}$; *UAS.RedStinger*: *Disc\RFP*$^{DsRedT4.UAS.Tag:NLS(tra)}$; *UAS.ovo*: *ovo*$^{svb.Scer\backslash UAS}$; *act>stop>d::EGFP*: *d*$^{FRT.Act5C.EGFP}$; *DE-cad::tomato*: *shg*$^{KI.T:Disc\backslash RFP\text{-}tdTomato}$; ds::EGFP: *Avic\GFP*$^{ds\text{-}EGFP}$; *hs.FLP*: *Scer\FLP1*$^{hs.PS}$; *sqh.UTRN::GFP*: *Hsap\UTRN*$^{Scer\backslash UAS.P\backslash T.T:Avic\backslash GFP\text{-}EGFP}$; *tub>stop>Gal4*: *Scer\GAL4*$^{FRT.Rnor\backslash Cd2.\alpha Tub84B}$.

Experimental Genotypes

(***Figure 1***) *w; DE-cad::tomato sqh.UTRN::GFP.*

(***Figure 1–figure supplement 1A***) *y w hs.FLP/ w; DE-cad::tomato/ UAS.GFP; hh.Gal4/ +.*

483 (***Figure 1–figure supplement 1B***) *y w hs.FLP/ w; DE-cad::tomato/ en.Gal4*
484 *UAS.act::GFP.*

485 (***Figure 2, Table 1***) *w; ds^{UA071} DE-cad::tomato sqh.UTRN::GFP/ DE-cad::tomato*
486 *sqh.UTRN::GFP; sr.Gal4/ UAS.ectoDs.*

487 (***Figure 3, Figure 4***) *w; ds::EGFP FRT40A.*

488 (***Figure 4–figure supplement 1***) *w; ds::EGFP FRT40A/ +; UAS.ectoDs/ sr.Gal4*
489 *UAS.RedStinger.*

490 (***Figure 5A,B, Figure 6***) *y w hs.FLP/ w; en.Gal4 UAS.DsRed/ +; act>stop>d::EGFP/ +.*

491 (***Figure 5C,D, Figure 5–figure supplement 1A, Figure 6***) *y w hs.FLP/ w; DE-*
492 *cad::tomato; act>stop>d::EGFP/ +.*

493 (***Figure 5–figure supplement 1B***) *y w hs.FLP/ w; ds^{UA071} ft^{15} DE-cad::tomato/ ds^{UA071};*
494 *act>stop>d::EGFP/ +.*

495 (***Figure 5–figure supplement 1C***) *y w hs.FLP/ w; ds^{UA071} ft^{15} DE-cad::tomato/ ft$^{G\text{-}rv}$;*
496 *act>stop>d::EGFP/ +.*

497 (***Figure 7, Figure 7–figure supplement 1***) *y w hs.FLP/ w; tub>stop>Gal4/ DE-*
498 *cad::tomato; UAS.ovo/ UAS.EB1::EGFP.*

499 (***Figure 8, Figure 8–figure supplement 1,3, Figure 8–movie supplement 1,2***) *y w*
500 *hs.FLP/ w; tub>stop>Gal4/ DE-cad::tomato; UAS.EB1::EGFP/ UAS.LifeAct::mCherry.*

501 ## Live Imaging of Larvae

502 To induce clones expressing *d::EGFP*, *ovo*, or *EB1::EGFP*, 2-4 h AEL embryos were
503 heat shocked on agar plates with fresh yeast paste at 33°C for 30 min in a water bath
504 (10-15 min for experiments in *ds*$^{-}$ and *ft*$^{-}$backgrounds). Larvae were grown at 25°C for
505 47-52 hr and moved to fresh standard food for 2-4 h (tagged Ds, D, and EB1) or 10-15
506 hr (predenticles) before imaging. Second stage larvae were washed in water and then
507 immobilised between a glass slide and coverslip by exploiting the surface tension of a
508 drop of Voltalef 10S oil or water. Epidermal cells in the A4-A7 abdominal segments of
509 the larvae were imaged live through the cuticle using a Leica SP5 inverted confocal
510 microscope with a 63x/1.4 oil immersion objective. Tagged fluorescent proteins were

511 excited sequentially with 488nm and 561nm laser beams and detected with 510-
512 540nm and 580-630nm emission filters, using Leica HyD hybrid detectors.

513 Quantification of Ds Amounts at Cellular Interfaces

514 Ds::EGFP membrane distribution was analysed in the apical plane of ventral
515 epidermal cells of early second stage larvae. Two juxtaposed areas of the segment (the
516 denticulate and undenticulate regions) were imaged separately to grant sufficient
517 resolution and subsequently merged, and maximum intensity projections of typically
518 4μm stacks were used to compensate for ruggedness in the denticulate region.
519 Between 3 and 12 images from different larvae were acquired and aligned to the
520 mediolateral axis using rows of tendon cells as reference. Ten straight lines parallel to
521 the anteroposterior axis and 4μm wide were drawn over the images at random
522 heights, and the profile of average fluorescence intensity along each line was plotted.
523 Each profile displayed peaks where the line intersected cell boundaries: the
524 fluorescence maxima were quantified using the BAR collection of ImageJ routines
525 (***Ferreira et al., 2017***) and manually assigned to the respective cellular interfaces. Due
526 to cell morphology and image noise not every line could provide a measure for each
527 interface, therefore for every image a value of mean intensity was calculated only for
528 cell boundaries intersected by at least 3 lines. The mean of means of all boundaries in
529 an image was used as reference to normalise the fluorescence intensity maxima.

530 Mapping of D polarity

531 D polarity at the plasma membrane was assessed over the whole segment by analysing
532 a total of 594 cells from small clones expressing *d::EGFP* in the ventral epidermis of 44
533 different larvae. Each cell was assigned a row number and polarity: rows of cells were
534 identifiable by proximity to conspicuous landmarks like denticles, sensory cells, and
535 tendons with unique shape, while polarity was scored based on whether D::EGFP
536 fluorescence was exclusively on the anterior (Ant) or posterior (Post) side of their
537 plasma membrane, unpolarised but clearly enriched at the membrane (Mem), or
538 homogeneously distributed in the cytoplasm (Cyt).

539 ## Analysis of Microtubule Growth Direction

540 Orientation of growing microtubules was analysed following EB1::EGFP comets in
541 ventral larval epidermal cells. Clonal expression of *EB1::EGFP* was necessary to avoid
542 interference from the strong signal of underlying muscle cells, and undenticulate
543 regions were preferred because denticles obscured the fluorescent signal. Early second
544 stage larvae were mounted in a small drop of water ensuring their posterior spiracles
545 were out of the liquid, and movies of individual cells were recorded at 5.16 s intervals
546 for typically 5 min, imaging a single 0.773μm apical confocal plane. Movie frames
547 were registered using the ImageJ plugin Stackreg (***Thevenaz et al., 1998***) to account
548 for slight movements of the larvae. Cells were then aligned to the mediolateral axis
549 using the T3 row of muscle attachment cells and rows of denticles as references, and
550 cells situated in the right hemisegments were flipped to match the mediolateral
551 orientation of the left hemisegment cells. Two cells, one in the A compartment (row 7
552 or 8) and one in the P (row -2 or -1), were selected from each of 10 larvae and pooled
553 for blind analysis. Comets were traced manually using the ImageJ plugin MtrackJ
554 (***Meijering et al., 2012***), sampling all the visible comets within each cell for as many
555 time points as were necessary to count 150-200 comets per cell, and angles of the
556 comets' trajectories relative to the anteroposterior axis of the larva were derived from
557 the first and last time point of their tracks.

558 ## Data Analysis

559 Data analysis was carried out in R 3.5.3 (***R Core Team, 2019***), using the *CircMLE*
560 (***Fitak and Johnsen, 2017***), *circular* (***Agostinelli and Lund, 2017***), *DescTools*
561 (***Signorell and mult. al., 2019***), *dplyr* (***Wickham et al., 2019***), *ggplot2* (***Wickham,***
562 ***2016***), and *mosaic* (***Pruim et al., 2017***) packages.

563 # ACKNOWLEDGEMENTS

564 We thank Jeffrey Axelrod and Katherine Sharp for kindly sharing data from the
565 Axelrod group (published in ***Olofsson et al., 2014; Sharp and Axelrod, 2016***), and
566 David Strutt, Eduardo Moreno, and the Bloomington Stock Center for flies. Our work
567 was supported by Wellcome Investigator Award 107060 to PAL.

COMPETING INTERESTS

The authors declare that no competing interests exist.

REFERENCES

Agostinelli, C., and Lund. (2017). R package 'circular': Circular Statistics (version 0.4-93). Retrieved from https://r-forge.r-project.org/projects/circular/

Akhmanova, A., and Steinmetz, M. O. (2008). Tracking the ends: a dynamic protein network controls the fate of microtubule tips. *Nature reviews. Molecular cell biology, 9*(4), 309-322. doi:10.1038/nrm2369

Ambegaonkar, A. A., and Irvine, K. D. (2015). Coordination of planar cell polarity pathways through Spiny-legs. *eLife, 4*, e09946. doi:10.7554/eLife.09946

Ambegaonkar, A. A., Pan, G., Mani, M., Feng, Y., and Irvine, K. D. (2012). Propagation of Dachsous-Fat planar cell polarity. *Current Biology, 22*(14), 1302-1308. doi:10.1016/j.cub.2012.05.049

Arata, M., Sugimura, K., and Uemura, T. (2017). Difference in Dachsous levels between migrating cells coordinates the direction of collective cell migration. *Developmental Cell, 42*(5), 479-497 e410. doi:10.1016/j.devcel.2017.08.001

Basler, K., and Struhl, G. (1994). Compartment boundaries and the control of Drosophila limb pattern by Hedgehog protein. *Nature, 368*(6468), 208-214. doi:10.1038/368208a0

Blair, S. S. (1995). Compartments and appendage development in Drosophila. *BioEssays, 17*(4), 299-309. doi:10.1002/bies.950170406

Bosveld, F., Bonnet, I., Guirao, B., Tlili, S., Wang, Z., Petitalot, A., Marchand, R., Bardet, P. L., Marcq, P., Graner, F., and Bellaiche, Y. (2012). Mechanical control of morphogenesis by Fat/Dachsous/Four-jointed planar cell polarity pathway. *Science, 336*(6082), 724-727. doi:10.1126/science.1221071

Brittle, A., Repiso, A., Casal, J., Lawrence, P. A., and Strutt, D. (2010). Four-jointed modulates growth and planar polarity by reducing the affinity of Dachsous for Fat. *Current Biology, 20*(9), 803-810. doi:10.1016/j.cub.2010.03.056

Brittle, A., Thomas, C., and Strutt, D. (2012). Planar polarity specification through asymmetric subcellular localization of Fat and Dachsous. *Current Biology, 22*(10), 907-914. doi:10.1016/j.cub.2012.03.053

Burute, M., and Kapitein, L. C. (2019). Cellular logistics: unraveling the interplay between microtubule organization and intracellular transport. *Annual Review of Cell and Developmental Biology, 35*, 29-54. doi:10.1146/annurev-cellbio-100818-125149

Casal, J., Lawrence, P. A., and Struhl, G. (2006). Two separate molecular systems, Dachsous/Fat and Starry night/Frizzled, act independently to confer planar cell polarity. *Development, 133*(22), 4561-4572. doi:10.1242/dev.02641

606 Casal, J., Struhl, G., and Lawrence, P. A. (2002). Developmental compartments and
607 planar polarity in *Drosophila*. *Current Biology, 12*(14), 1189-1198.
608 doi:10.1016/s0960-9822(02)00974-0

609 Delon, I., Chanut-Delalande, H., and Payre, F. (2003). The Ovo/Shavenbaby
610 transcription factor specifies actin remodelling during epidermal
611 differentiation in *Drosophila*. *Mechanisms of Development, 120*(7), 747-758.
612 doi:10.1016/s0925-4773(03)00081-9

613 Diaz-Benjumea, F. J., and Cohen, S. M. (1995). Serrate signals through Notch to
614 establish a Wingless-dependent organizer at the dorsal/ventral compartment
615 boundary of the *Drosophila* wing. *Development, 121*(12), 4215-4225. Retrieved
616 from https://www.ncbi.nlm.nih.gov/pubmed/8575321

617 Doherty, D., Feger, G., Younger-Shepherd, S., Jan, L. Y., and Jan, Y. N. (1996). Delta is
618 a ventral to dorsal signal complementary to Serrate, another Notch ligand, in
619 *Drosophila* wing formation. *Genes & Development, 10*(4), 421-434.
620 doi:10.1101/gad.10.4.421

621 Donoughe, S., and DiNardo, S. (2011). *dachsous* and *frizzled* contribute separately to
622 planar polarity in the Drosophila ventral epidermis. *Development, 138*(13),
623 2751-2759. doi:10.1242/dev.063024

624 Ferreira, T., Hiner, M., Rueden, C., Miura, K., Eglinger, J., and Chef, B. (2017). BAR
625 1.5.1. Retrieved from https://doi.org/10.5281/zenodo.495245

626 Fitak, R. R., and Johnsen, S. (2017). Bringing the analysis of animal orientation data
627 full circle: model-based approaches with maximum likelihood. *The Journal of*
628 *Experimental Biology, 220*(Pt 21), 3878-3882. doi:10.1242/jeb.167056

629 Fulford, A. D., and McNeill, H. (2019). Fat/Dachsous family cadherins in cell and
630 tissue organisation. *Current Opinion in Cell Biology, 62*, 96-103.
631 doi:10.1016/j.ceb.2019.10.006

632 Gomez, J. M., Chumakova, L., Bulgakova, N. A., and Brown, N. H. (2016).
633 Microtubule organization is determined by the shape of epithelial cells. *Nature*
634 *Communications, 7*, 13172. doi:10.1038/ncomms13172

635 Hale, R., Brittle, A. L., Fisher, K. H., Monk, N. A., and Strutt, D. (2015). Cellular
636 interpretation of the long-range gradient of Four-jointed activity in the
637 *Drosophila* wing. *eLife, 4*, e05789. doi:10.7554/eLife.05789

638 Harumoto, T., Ito, M., Shimada, Y., Kobayashi, T. J., Ueda, H. R., Lu, B., and Uemura,
639 T. (2010). Atypical cadherins Dachsous and Fat control dynamics of
640 noncentrosomal microtubules in planar cell polarity. *Developmental Cell,*
641 *19*(3), 389-401. doi:10.1016/j.devcel.2010.08.004

642 Ishikawa, H. O., Takeuchi, H., Haltiwanger, R. S., and Irvine, K. D. (2008). Four-
643 jointed is a Golgi kinase that phosphorylates a subset of cadherin domains.
644 *Science, 321*(5887), 401-404. doi:10.1126/science.1158159

645 Lawrence, P. A., and Casal, J. (2018). Planar cell polarity: two genetic systems use one
646 mechanism to read gradients. *Development, 145*(23). doi:10.1242/dev.168229

Lawrence, P. A., and Struhl, G. (1996). Morphogens, compartments, and pattern: lessons from *Drosophila*? *Cell, 85*(7), 951-961. doi:10.1016/s0092-8674(00)81297-0

Ma, D., Yang, C. H., McNeill, H., Simon, M. A., and Axelrod, J. D. (2003). Fidelity in planar cell polarity signalling. *Nature, 421*(6922), 543-547. doi:10.1038/nature01366

Mao, Y., Rauskolb, C., Cho, E., Hu, W. L., Hayter, H., Minihan, G., Katz, F. N., and Irvine, K. D. (2006). Dachs: an unconventional myosin that functions downstream of Fat to regulate growth, affinity and gene expression in *Drosophila*. *Development, 133*(13), 2539-2551. doi:10.1242/dev.02427

Matakatsu, H., and Blair, S. S. (2004). Interactions between Fat and Dachsous and the regulation of planar cell polarity in the *Drosophila* wing. *Development, 131*(15), 3785-3794. doi:10.1242/dev.01254

Matis, M., and Axelrod, J. D. (2013). Regulation of PCP by the Fat signaling pathway. *Genes & Development, 27*(20), 2207-2220. doi:10.1101/gad.228098.113

Matis, M., Russler-Germain, D. A., Hu, Q., Tomlin, C. J., and Axelrod, J. D. (2014). Microtubules provide directional information for core PCP function. *eLife, 3*, e02893. doi:10.7554/eLife.02893

Meijering, E., Dzyubachyk, O., and Smal, I. (2012). Methods for cell and particle tracking. *Methods in Enzymology, 504*, 183-200. doi:10.1016/B978-0-12-391857-4.00009-4

Olofsson, J., Sharp, K. A., Matis, M., Cho, B., and Axelrod, J. D. (2014). Prickle/spiny-legs isoforms control the polarity of the apical microtubule network in planar cell polarity. *Development, 141*(14), 2866-2874. doi:10.1242/dev.105932

Picone, R., Ren, X., Ivanovitch, K. D., Clarke, J. D., McKendry, R. A., and Baum, B. (2010). A polarised population of dynamic microtubules mediates homeostatic length control in animal cells. *PLoS Biology, 8*(11), e1000542. doi:10.1371/journal.pbio.1000542

Pruim, R., Kaplan, D. T., and Horton, N. J. (2017). The mosaic Package: Helping Students to 'Think with Data' Using R. *The R Journal, 9*(1), 77--102. Retrieved from https://journal.r-project.org/archive/2017/RJ-2017-024/index.html

R Core Team. (2019). R: A Language and Environment for Statistical Computing. Vienna, Austria: R Foundation for Statistical Computing. Retrieved from https://www.R-project.org/

Repiso, A., Saavedra, P., Casal, J., and Lawrence, P. A. (2010). Planar cell polarity: the orientation of larval denticles in *Drosophila* appears to depend on gradients of Dachsous and Fat. *Development, 137*(20), 3411-3415. doi:10.1242/dev.047126

Rogulja, D., Rauskolb, C., and Irvine, K. D. (2008). Morphogen control of wing growth through the Fat signaling pathway. *Developmental Cell, 15*(2), 309-321. doi:10.1016/j.devcel.2008.06.003

Rovira, M., Saavedra, P., Casal, J., and Lawrence, P. A. (2015). Regions within a single epidermal cell of *Drosophila* can be planar polarised independently. *eLife, 4*, e06303. doi:10.7554/eLife.06303

690 Saavedra, P., Brittle, A., Palacios, I. M., Strutt, D., Casal, J., and Lawrence, P. A. (2016).
691 Planar cell polarity: the Dachsous/Fat system contributes differently to the
692 embryonic and larval stages of *Drosophila*. *Biology Open, 5*(4), 397-408.
693 doi:10.1242/bio.017152

694 Saavedra, P., Vincent, J. P., Palacios, I. M., Lawrence, P. A., and Casal, J. (2014).
695 Plasticity of both planar cell polarity and cell identity during the development
696 of *Drosophila*. *eLife, 3*, e01569. doi:10.7554/eLife.01569

697 Schuyler, S. C., and Pellman, D. (2001). Microtubule "plus-end-tracking proteins": The
698 end is just the beginning. *Cell, 105*(4), 421-424. doi:10.1016/s0092-
699 8674(01)00364-6

700 Sharp, K. A., and Axelrod, J. D. (2016). Prickle isoforms control the direction of tissue
701 polarity by microtubule independent and dependent mechanisms. *Biology*
702 *Open, 5*(3), 229-236. doi:10.1242/bio.016162

703 Shimada, Y., Yonemura, S., Ohkura, H., Strutt, D., and Uemura, T. (2006). Polarized
704 transport of Frizzled along the planar microtubule arrays in *Drosophila* wing
705 epithelium. *Developmental Cell, 10*(2), 209-222.
706 doi:10.1016/j.devcel.2005.11.016

707 Signorell, A., and mult. al. (2019). DescTools: Tools for Descriptive Statistics.
708 Retrieved from https://cran.r-project.org/package=DescTools

709 Simon, M. A., Xu, A., Ishikawa, H. O., and Irvine, K. D. (2010). Modulation of
710 Fat:dDchsous binding by the cadherin domain kinase Four-jointed. *Current*
711 *Biology, 20*(9), 811-817. doi:10.1016/j.cub.2010.04.016

712 Singh, A., Saha, T., Begemann, I., Ricker, A., Nusse, H., Thorn-Seshold, O., Klingauf,
713 J., Galic, M., and Matis, M. (2018). Polarized microtubule dynamics directs cell
714 mechanics and coordinates forces during epithelial morphogenesis. *Nature*
715 *Cell Biology, 20*(10), 1126-1133. doi:10.1038/s41556-018-0193-1

716 Sison, C. P., and Glaz, J. (1995). Simultaneous confidence intervals and sample size
717 determination for multinomial proportions. *Journal of the American Statistical*
718 *Association, 90*(429), 366-369. doi:10.1080/01621459.1995.10476521

719 Struhl, G., Barbash, D. A., and Lawrence, P. A. (1997). Hedgehog organises the pattern
720 and polarity of epidermal cells in the *Drosophila* abdomen. *Development,*
721 *124*(11), 2143-2154. Retrieved from
722 https://www.ncbi.nlm.nih.gov/pubmed/9187141

723 Tabata, T., and Takei, Y. (2004). Morphogens, their identification and regulation.
724 *Development, 131*(4), 703-712. doi:10.1242/dev.01043

725 Thevenaz, P., Ruttimann, U. E., and Unser, M. (1998). A pyramid approach to
726 subpixel registration based on intensity. *IEEE Transactions on Image*
727 *Processing 7*(1), 27-41. doi:10.1109/83.650848

728 Thurmond, J., Goodman, J., Strelets, V., Attrill, H., Gramates, L., Marygold, S.,
729 Matthews, B., Millburn, G., Antonazzo, G., Trovisco, V., Kaufman, T., .BR, C.,
730 and and the FlyBase Consortium. (2019). FlyBase 2.0: the next generation.
731 *Nucleic Acids Research, 47*, D759–D765.

Umetsu, D., Aigouy, B., Aliee, M., Sui, L., Eaton, S., Julicher, F., and Dahmann, C. (2014). Local increases in mechanical tension shape compartment boundaries by biasing cell intercalations. *Current Biology, 24*(15), 1798-1805. doi:10.1016/j.cub.2014.06.052

Walters, J. W., Dilks, S. A., and DiNardo, S. (2006). Planar polarization of the denticle field in the *Drosophila* embryo: roles for Myosin II (*zipper*) and *fringe*. *Developmental Biology, 297*(2), 323-339. doi:10.1016/j.ydbio.2006.04.454

Wickham, H. (2016). *ggplot2: Elegant Graphics for Data Analysis*: Springer-Verlag New York.

Wickham, H., François, R., Henry, L., and Müller, K. (2019). dplyr: A Grammar of Data Manipulation. Retrieved from https://CRAN.R-project.org/package=dplyr

745 # FIGURE LEGENDS

746 **Figure 1.** Predenticles and Ds activity landscape. (**A**) Ventral denticulate area of a mid
747 second stage larva. Predenticles (rows 0 to 6) and muscle attachment cells (tendon
748 rows T1 and T2) are marked in green (UTRN::GFP, labelling actin), and cell
749 boundaries in magenta (DE-cad::tomato). The rows are not completely regular; here,
750 one T2 cell contacts two row 6 cells at the posterior (asterisk) — typically, T2 only
751 contacts row 5 cells. (**B**) Model of the landscape of Ds and Fj and therefore of PCP in
752 the wild type (***Rovira et al., 2015; Saavedra et al., 2016***). In T1 and T2 a low level of
753 *ds* expression together with a high level of Fj reduces Ds activity in the cells affected.
754 The sloped line in each cell indicates different amounts of Ds activity at its anterior
755 and posterior limits, the direction of the slope correlating with the cell's polarity.
756 Denticle polarity is shown below and is a readout of the zigzag landscape of Ds
757 activity: each cell points its denticles towards the neighbour with the higher Ds
758 activity. Two rows of the P compartment are highlighted in blue, tendon cells are
759 shaded in grey. Anterior is to the left in all figures. Scale bar: 20μm.

760

761 **Figure 1—figure supplement 1.** Larval ventral abdomen. Overview of segments with
762 some cells expressing GFP under the control of the promoters of (**A**) *hedgehog* or (**B**)
763 *engrailed*, both markers of the P compartment (***Blair, 1995; Lawrence and Struhl,***
764 ***1996***). GFP labels four rows of cells, between the most posterior row of the A
765 compartment (identified by sensory cells, S) and the most anterior row of the
766 following segment (tendon cells T1, see ***Saavedra et al., 2014***). Cell outlines and
767 denticles are labelled in magenta (DE-cad::tomato). (**A**) *hh.Gal4* marks very sharply
768 the front of the P compartment, but its expression is weak in the posterior denticulate
769 cells. (**B**) *en.Gal4* on the contrary indicates precisely the rear edge of the P
770 compartment, but occasionally also weakly labels a few cells at the back of the A
771 compartment (asterisks). A, anterior compartment. P, posterior compartment. S,
772 sensory cells. T3, tendon cell row that has distinctly elongated cells. Scale bars: 20μm.

773

774 **Figure 2.** PCP and atypical cells in polarity modified larvae. Denticulate areas of
775 polarity modified larvae: (**A-C**) typical cells, (**D-F**) an atypical cell in row 4 (having
776 two posterior neighbours with different Ds activity), and (**G-I**) an atypical cell in row
777 2 (having two anterior neighbours with different Ds activity). Predenticles and
778 denticles in rows 1, 2 and 4, 5 with polarity opposite from wildtype are highlighted in
779 magenta. (**A,D,G**) Images of predenticles, tendon cells, and cell boundaries labelled as
780 in ***Figure 1A***. (**B,E,H**) Schemes of cell outlines and predenticle orientation. (**C,F,I**)
781 Models of modified *ds* expression, Ds activity landscape and denticle polarity in cross
782 sections taken at the dotted blue lines in **B,E,H**. Blue shading indicates P
783 compartment cells, grey denotes tendon cells, magenta marks the atypical cell. Note
784 that, contrary to wildtype (***Rovira et al., 2015***), in polarity modified larvae row 4
785 atypical cells are monopolar (**D,E**), while row 2 atypical cells are multipolar (**G,H**).
786 For quantitation of predenticle polarity in row 4 and row 2 atypical cells of wild type
787 and polarity modified larvae, see ***Table 1***. Scale bars: 20μm.

788

789 **Figure 3.** Ds localisation in the larval ventral abdomen. Larvae expressing *ds*::EGFP
790 from the tagged endogenous *ds* locus (***Brittle et al., 2012***) show a ubiquitous punctate
791 pattern of fluorescence that concentrates on plasma membranes. (**A**) Denticulate and
792 (**B**) undenticulate areas of early second stage larvae; the cell rows exhibit no obvious
793 differences in *ds* expression or distribution, with the exception of the strong signal
794 around T3 tendon cells. (**C**) Detail of Ds localisation in puncta at the cell membrane. 0
795 to 6, denticle cell rows. 7 to -2, undenticulate cell rows. S, sensory cell. T1, T2, T3,
796 tendon cell rows. Scale bars: 20μm (**A,B**), 10μm (**C**).

797

798 **Figure 4.** Quantitation of Ds levels at cellular interfaces across the segment. (**Top**) Dot
799 plot of normalised fluorescence intensity maxima corresponding to amounts of Ds at
800 boundaries between cell rows of the larval ventral abdomen. Data are pooled from 12
801 (denticulate area) and 5 (undenticulate area) images of different larvae. Mean value
802 and 95% confidence interval for each interface are indicated in red. Letters arise from
803 Tukey's multiple comparison test between all interfaces; means of interfaces with the
804 same letter are not significantly different ($p>0.05$). The graph shows no evidence for a

segment-wide gradient of Ds accumulation at the cell membranes, however the 9/T3 and T3/10 boundaries are significantly different from all others, indicating a clear peak in front of the A/P boundary. (**Middle**) Diagram of denticle polarity, as in ***Figure 1B***. Sensory cells identify rows 8 and 11. (**Bottom**) Comparisons between Ds amounts at posterior and anterior interfaces of each cell row. Differences in mean normalised fluorescence at the opposite sides of a cell are calculated with 95% confidence interval by Tukey's test. Red indicates a significant difference. Note the significant and opposite differences in cell rows 9 and 10, highlighting the presence of a fluorescence peak around T3.

Figure 4—figure supplement 1. Quantitation of Ds levels at cellular interfaces in polarity modified larvae. Dot plot, diagram of denticle polarity, and pairwise comparisons are presented as in ***Figure 4***. Data are pooled from 3 images of larvae where overexpression of untagged Ds is specifically driven in tendons and changes the polarity of adjacent denticle cells (see ***Figure 2***). Ds distribution in polarity modified larvae is visibly altered, reflecting the predicted changes in the landscape of Ds activity. For example, more untagged Ds in T1 attracts more Ft molecules in row 2 cells to the T1/2 boundary, consequently displacing the row 2 endogenous, tagged Ds to the 2/3 boundary and raising fluorescence on that interface. The same effect emanating anteriorly from T2 raises Ds fluorescence at the 3/4 boundary. As expected, Ds amounts on the 2/3 and 3/4 boundaries are significantly higher than on the surrounding boundaries, arguing that the method is capable of detecting cellular interfaces with raised Ds activity.

Figure 5. D polarity at the plasma membrane in small clones. (**A**) Several cells of the A compartment expressing *d::EGFP*: in row 4, where denticles point anteriorly, D is mostly on the posterior membrane; in rows 5, 6 and 7, with posterior-pointing polarity, D accumulates instead at the front of the cells. Round or comma-like structures are due to autofluorescence from overlying denticles. (**B**) A posterior cell (row -2) accumulates D at its rear, arguing for anterior-pointing polarity. P compartment is labelled in magenta by en.Gal4 UAS.DsRed. (**C**) Cells of rows 10 and

836 11, where D localises on the anterior and posterior sides of the plasma membrane,
837 respectively (see ***Figure 5—figure supplement 1A*** for cell outlines). (**D**) Row 10 cell
838 with more D on the front side of the cell membrane, suggesting its polarity points
839 backwards. The sensory cell process associated with row 11 also expresses *d::EGFP*,
840 and as with other cells from row 11 has most D at the posterior side. S, sensory cell.
841 Scale bars: 10μm.

842

843 **Figure 5—figure supplement 1.** D localisation on limited parts of the plasma
844 membrane, and in *ds*⁻ and *ft*⁻ larvae. (**A**) Row 10 and 11 cells from a wildtype larva
845 expressing *d::EGFP*, with cell outlines marked in magenta by DE-cad::tomato (see
846 ***Figure 5C*** for single EGFP channel). D is on just one side of each cell, but its
847 localisation at the plasma membrane is not continuous: the row 10 cell accumulates D
848 on the anterior membrane only where it confronts a T3 cell, not where it faces other
849 row 10 cells; the row 11 cell has D localised at its back, but only where it contacts row
850 -2 cells. (**B**) Cells of the A compartment expressing *d::EGFP* in *ds*⁻ background. D is
851 localised asymmetrically, although less markedly than in wildtype and sometimes with
852 opposite polarity (e.g. cells in row 9). (**C**) Anterior cells expressing *d::EGFP* in *ft*⁻
853 background. D localisation resembles that of *ds*⁻ larvae: it can be asymmetrical and
854 sometimes has polarity opposite to wildtype (e.g. cells in row 8). Scale bars: 10μm.

855

856 **Figure 6.** The localisation of D cell by cell. D localisation in all the cell rows, derived
857 from the analysis of small clones expressing *d::EGFP*. Cells where D accumulates on
858 just the anterior side of the plasma membrane contribute to red circles, cells where D
859 is only on the posterior side to blue circles, and cells where polarity is unscorable to
860 grey circles. The position of each circle denotes the cell row and percentage of cells
861 with the indicated polarity in that row; circle area is proportional to the number of
862 cells represented. Since D is thought to accumulate on the side of a cell facing the
863 neighbour with the least Ds, the pattern of D polarity in the undenticulate region
864 suggests that there is a peak of Ds activity in row 10 (see ***Figure 9*** for full model). Ant,
865 anterior D polarity. Cyt, cytoplasmic D localisation. Mem, membrane accumulation of
866 D but no asymmetry. Post, posterior D polarity. n = 594 cells from 44 larvae.

867

868 **Figure 7.** *ovo*-overexpressing clones in normally undenticulate areas of the epidermis.
869 (**A**) Clone in the A compartment (cell rows 7, 8, and 9), marked with EGFP and
870 producing ectopic denticles that point backwards. (**B**) Clone in the P compartment
871 (cell row -1), ectopic denticles pointing forwards. Note that denticles are produced
872 somewhat sporadically and that denticle numbers vary per cell. Scale bars: 10μm.

873

874 **Figure 7—figure supplement 1.** Unusual *ovo*-expressing clones with ambiguous
875 polarity in row 11 cells. (**A,B**) Clones marked with EGFP and producing ectopic
876 denticles in rows 10 and 11. DE-cad::tomato (magenta) labels cell boundaries and
877 denticles, which in this area can be tenuous and hard to discern. (**A',B'**) Schemes of
878 cell outlines and denticle orientation; denticles with uncharacteristic polarity are
879 highlighted in red. (**A,A'**) Denticles pointing in opposite directions in two contiguous
880 row 11 cells; all denticles in the neighbouring row 10 cells point backwards. (**B,B'**)
881 Denticles pointing in mixed directions within a single row 11 cell. Scale bars: 10μm.

882

883 **Figure 8.** Analysis of microtubule polarity in larval epidermal cells. (**A,B**) Rose
884 diagrams showing the distribution of growing microtubule direction in cells of the (**A**)
885 anterior and (**B**) posterior compartment. EB1 comets are grouped in bins of 4 degrees,
886 the length of each bin indicating the percentage of comets with a specific orientation.
887 Comets pointing to the left (180°) grow anteriorly, comets pointing to the right (0°)
888 posteriorly, up (90°) are medial, and down (270°) are lateral; n is the total number of
889 comets tracked, from the number of cells/larvae indicated in parenthesis. (**C,D**)
890 Frequency of microtubules with either anterior, posterior, medial or lateral
891 orientation in (**C**) A cells and (**D**) P cells. Comets are sorted into four sectors of 90
892 degrees centred on the anteroposterior and mediolateral axes. The 95% confidence
893 interval for all comets in each quadrant is calculated according to ***Sison and Glaz***
894 (***1995***). (**E**) Dot plot comparing the orientation of microtubules within each cell of the
895 A and P compartment. For every cell, the fraction of comets falling into the anterior
896 quadrant is plotted next to the fraction in the posterior quadrant, medial next to
897 lateral. Lines connecting the twin values from the same cell emphasise the high

variability between individuals. Mean percentage and 95% confidence interval of the mean for each set of cells are shown. Overlying numbers display the exiguous difference between means of the anterior versus posterior and medial versus lateral quadrants, with 95% confidence interval estimated by recalculating the difference of the means after resampling the data 10,000 times and finding the 0.025 and 0.975 quantiles of the resulting set of values.

Figure 8—figure supplement 1. Local polarity biases in microtubule growth. P values of chi-squared tests between numbers of comets whose orientation falls in opposite 22.5 degree sectors. Tables display the number of comets per sector and p values for larval and pupal sets of A and P cells. Sectors centred on the anteroposterior axis are highlighted in green.

Figure 8—figure supplement 2. Analysis of microtubule polarity in cells of the pupal abdomen, based on raw data kindly provided by the Axelrod group. (**A-E**) Rose diagrams of microtubule growth distribution, frequencies of comet orientation, and dot plot of microtubule direction in individual cells are presented as in ***Figure 8***. (**A,C,E**) Anterior pupal cells, (**B,D,E**) posterior pupal cells. n indicates total number of comets analysed, from the amount of pupae specified in parenthesis. Unlike ours, the data acquired by Axelrod's group contain no information about which hemisegment they were sampled from; comet orientation is still classified as medial and lateral to facilitate comparison with our results, however these categories should be considered with caution. Note that, in contrast with larval data where differences between the frequencies of comets in opposite quadrants are not statistically significant (***Figure 8C,D***), in pupae there are significant biases in the proportion of anteriorly/posteriorly and medially/laterally growing microtubules (see non-overlapping confidence intervals in **C** and **D**).

Figure 8—figure supplement 3. Maximum likelihood best models of microtubule angular distributions. Using a maximum likelihood approach (***Fitak and Johnsen,***

928 ***2017***) we plot the angular distribution of all growing microtubules and the best fit is to
929 bimodal distributions with two peaks near 180 degrees apart in the mediolateral axis.
930 The distribution densities are shown in blue (darker blue representing the anterior
931 and posterior 90 degree quadrants). A circular histogram (bin size 22.5 degree) of the
932 angle data is at the centre of each plot in grey. The mean vector is shown in red and
933 the two mean angles are shown with discontinuous arrows. The mean values (θ)
934 concentration parameters (κ), proportional size of the first distribution (λ), mean
935 vector angle ($\bar{\theta}$) and dispersion ($\bar{R}$) are shown below each plot. A deviation of 10
936 degrees in one of the peaks of the distribution from the true mediolateral axis is
937 enough to create a difference in the density area of the anterior and posterior
938 quadrants. In both larval and pupal sets of A cells the area of the posterior quadrant
939 density is slightly bigger (red arrowhead) than the anterior one (green arrowhead). In
940 both larval and pupal sets of P cells the area of the anterior quadrant is slightly bigger
941 (red arrowhead) than the posterior one (green arrowhead).

942

943 **Figure 8—movie supplement 1.** Film of microtubule dynamics in a representative
944 larval A cell. EB1::GFP comets in a row 7 cell from the right hemisegment imaged for
945 4 minutes at 5.16 s intervals. Juxtaposed movie shows manual tracing of 200 comet
946 trajectories over the entire surface of the cell. Anterior is to the left, medial is down.
947 Scale bar: 5μm.

948

949 **Figure 8—movie supplement 2.** Film of microtubule dynamics in a representative
950 larval P cell. EB1::GFP comets in a row -1 cell from the left hemisegment imaged for 4
951 minutes at 5.16 s intervals. Juxtaposed movie shows manual tracing of 200 comet
952 trajectories over the entire surface of the cell. Anterior is to the left, medial is up. Scale
953 bar: 5μm.

954

955 **Figure 9.** Model of Ds activity and planar cell polarity in the larval ventral epidermis.
956 The strong Ds accumulation on both sides of T3 tendon cells (***Figures 3*** and ***4***)
957 suggests that *ds* expression is high in T3 itself and/or its neighbours. In addition,

958 D::EGFP clones (***Figures 5*** and ***6***) and ectopic denticles (***Figure7—figure supplement***
959 ***1A***) show that polarity of row 10 points backwards, away from T3, implying that Ds
960 activity is higher in row 11 than in T3. These two observations combined argue that *ds*
961 expression peaks in row 10, two cells in front of the A/P border, with Ds activity also
962 high in T3 and row 11. Graded *ds* expression forwards and backwards from this peak
963 and high levels of *fj* expression in tendon cells determine the landscape of Ds activity,
964 now extended to the undenticulate region. The differences in Ds activity between each
965 cell's anterior and posterior sides orient D accumulation; D localises to the side that
966 has the highest Ds activity and "sees" the lowest Ds activity in its neighbour. D
967 asymmetrical distribution precisely matches the pattern of cell polarity revealed by
968 denticles, as demonstrated by direct visualisation of tagged D in the whole segment
969 and induction of denticles in normally naked cells. Blue shading indicates P
970 compartment cells, grey shading tendons.

971

Table 1 Atypical cells: quantitation of predenticle polarities in relation to neighbouring cells, showing the effect of over expressing *ds* in the Tendon cells.

wild type

Anterior neighbour	Predenticle polarity of atypical Row 2 cells		Posterior neighbour
	Anteriorly	Posteriorly	
T1 cell	0	**44***	Row 3 cell
Row 2 cell	0	**52***	Row 3 cell

Predenticles of 39 atypical cells from 15 larvae. Fischer's exact test p-value = 1. *8 preden-ticles with an unclear position were allocated equally to these groups.

Anterior neighbour	Predenticle polarity of atypical Row 4 cells		Posterior neighbour
	Anteriorly	Posteriorly	
Row 3 cell	**207**	0	T2 cell
Row 3 cell	105*	**45**	Row 4 cell

Predenticles of 74 atypical cells from 21 larvae. Fischer's exact test p-value < 2.2^{-16}. *18 pre-denticles with an unclear position were arbitrarily added to this class, in favour of the null hypothesis.

sr.Gal4 UAS.EctoDs

Anterior neighbour	Predenticle polarity of atypical Row 2 cells		Posterior neighbour
	Anteriorly	Posteriorly	
T1 cell	**61**	8*	Row 3 cell
Row 2 cell	7**	**49**	Row 3 cell

Predenticles of 42 atypical cells from 28 larvae. Fischer's exact test p-value <2.2^{-16}. *6 and **3 predenticles with an unclear position were arbitrarily added to these classes.

Anterior neighbour	Predenticle polarity of atypical Row 4 cells		Posterior neighbour
	Anteriorly	Posteriorly	
Row 3 cell	5	**119***	T2 cell
Row 3 cell	0	**99***	Row 4 cell

Predenticles of 40 atypical cells from 20 larvae. Fischer's exact test p-value = 0.068. *14 predenticles with an unclear position were allocated equally to these groups.

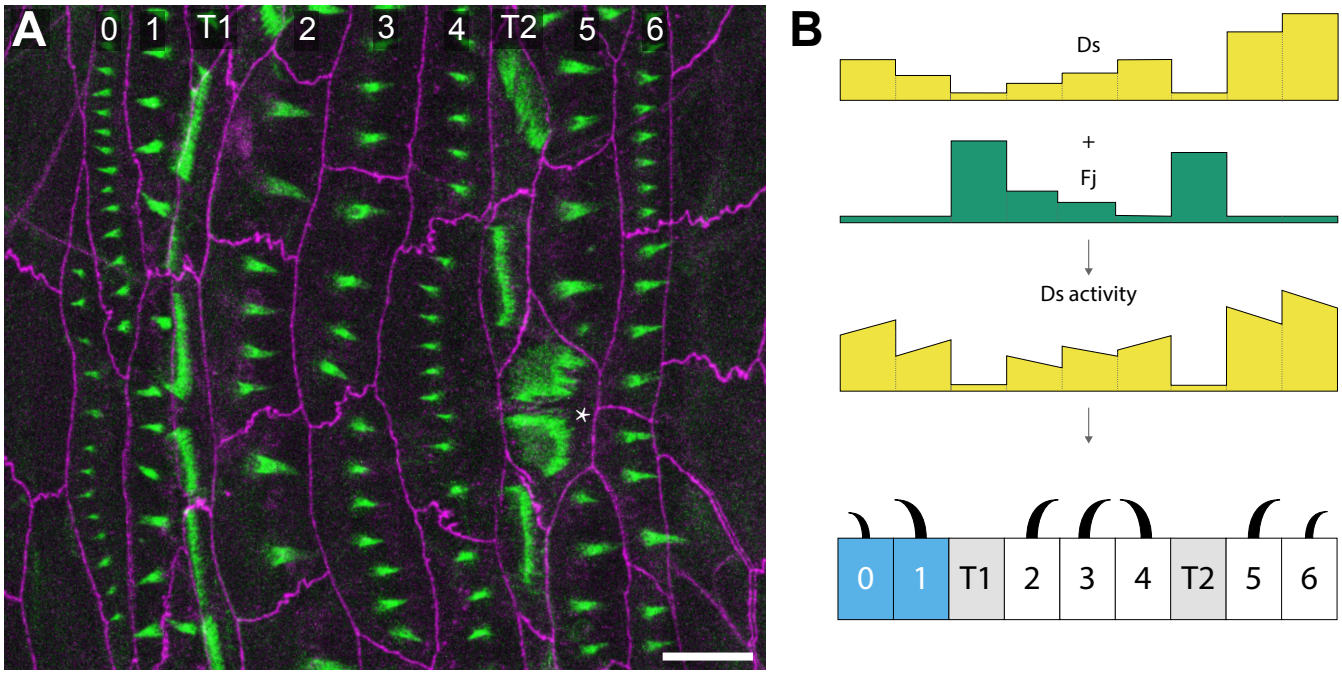

Pietra et al. Figure 1

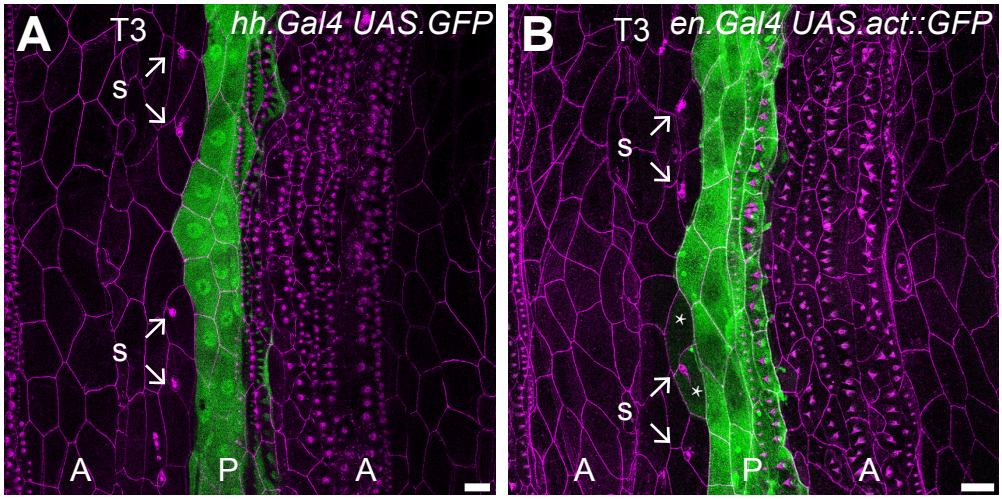

Pietra et al. Figure 1–figure supplement 1

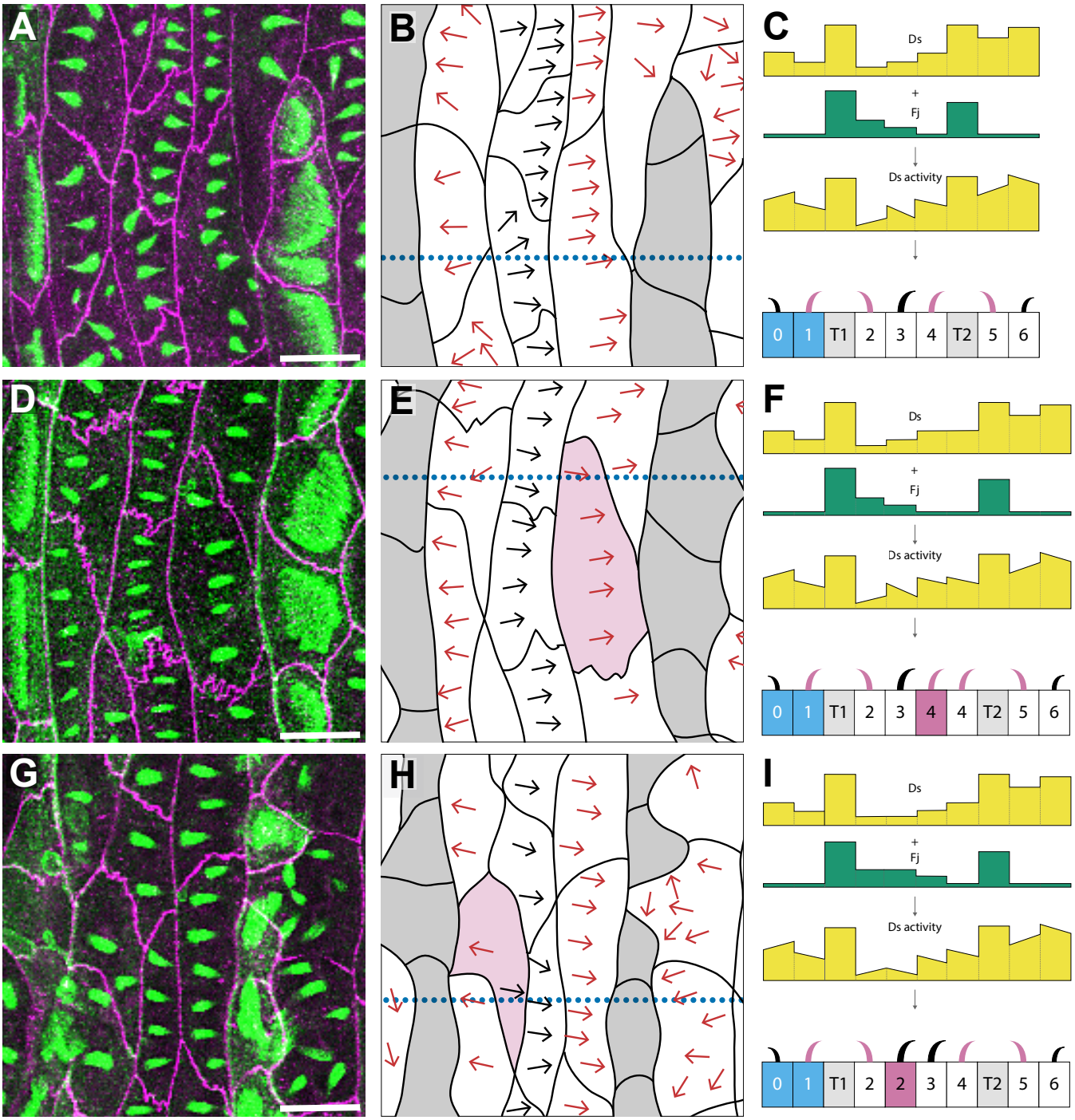

Pietra et al. Figure 2

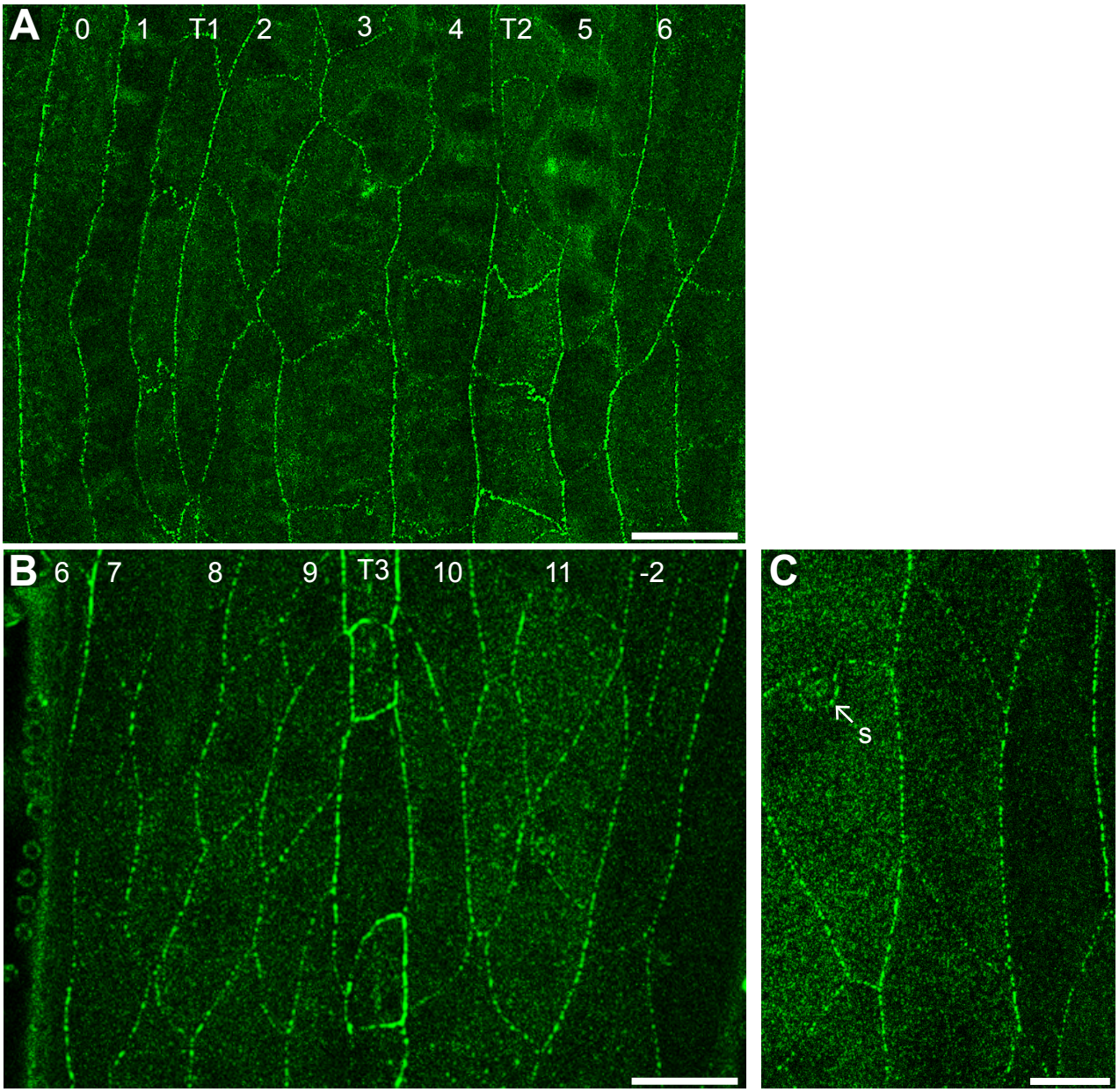

Pietra et al. Figure 3

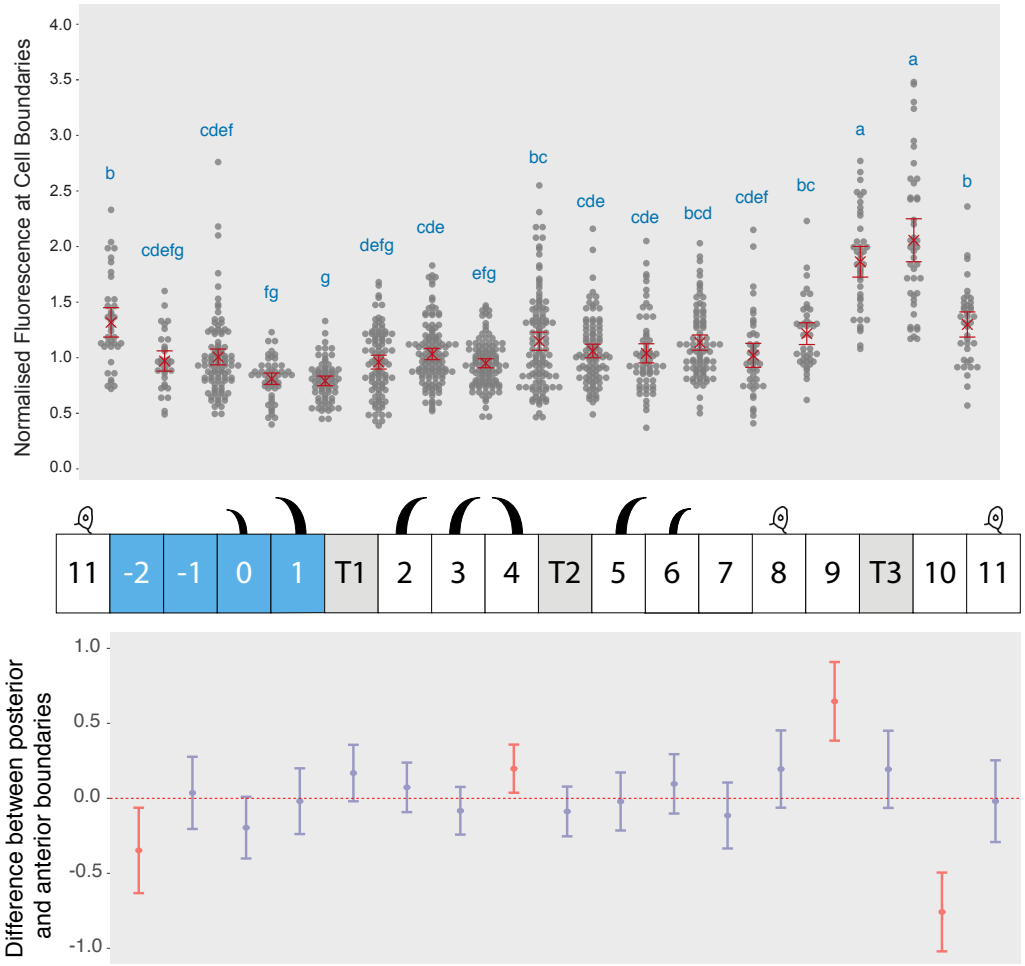

Pietra et al. Figure 4

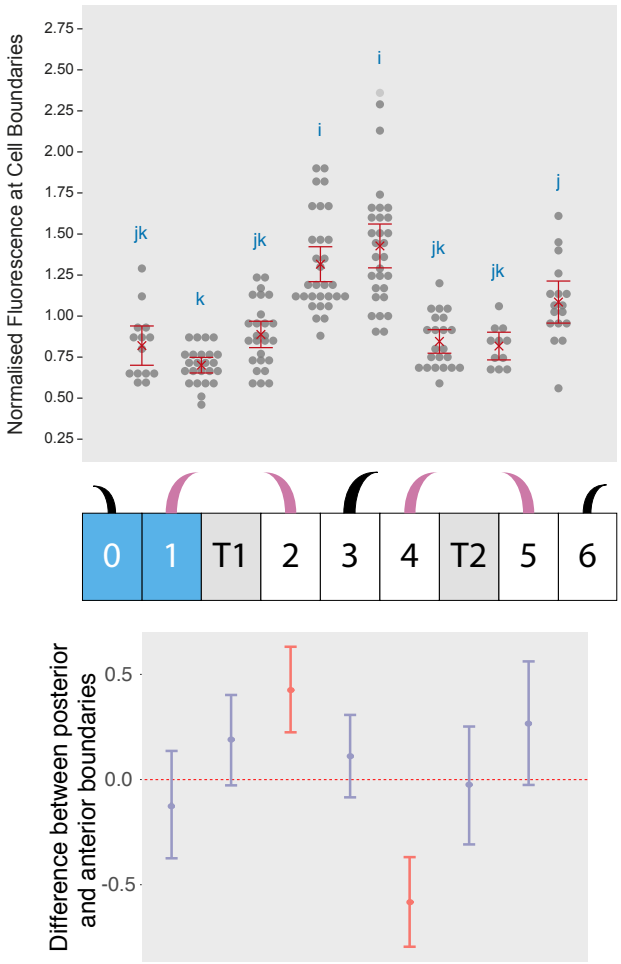

Pietra et al. Figure 4–figure supplement 1

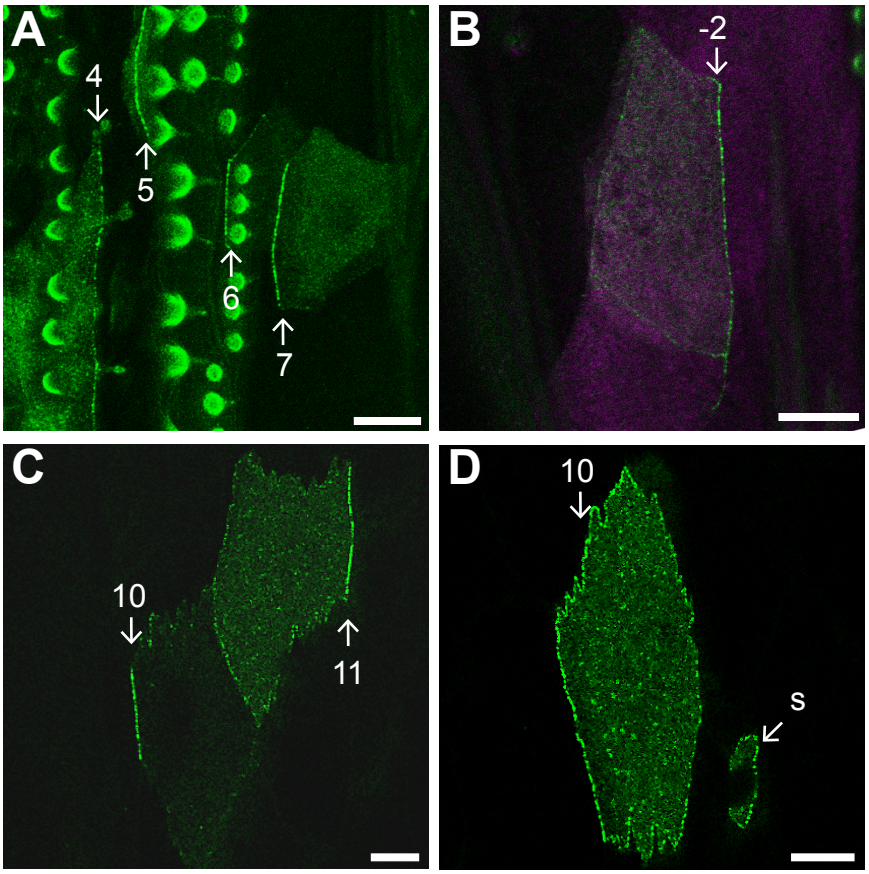

Pietra et al. Figure 5

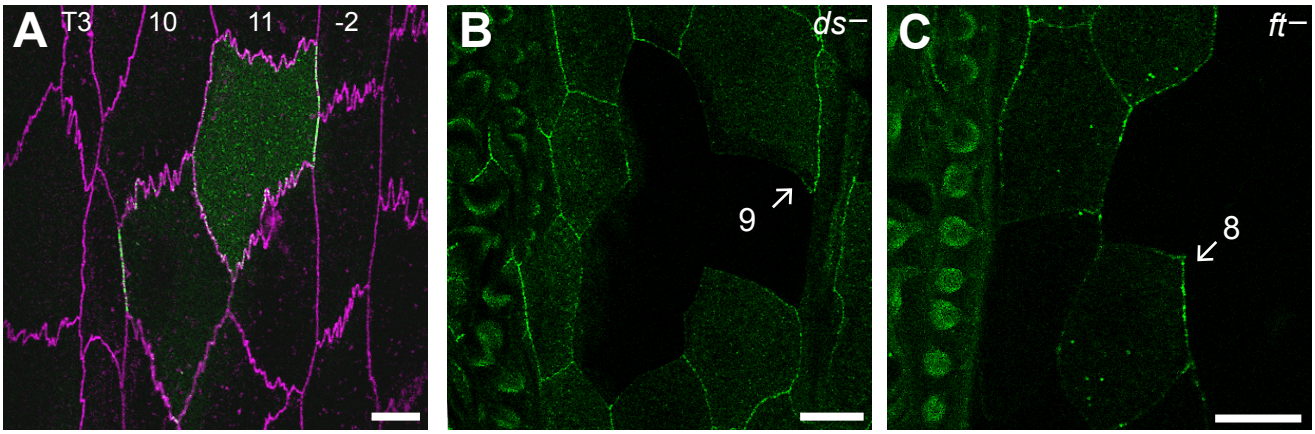

Pietra et al. Figure 5–figure supplement 1

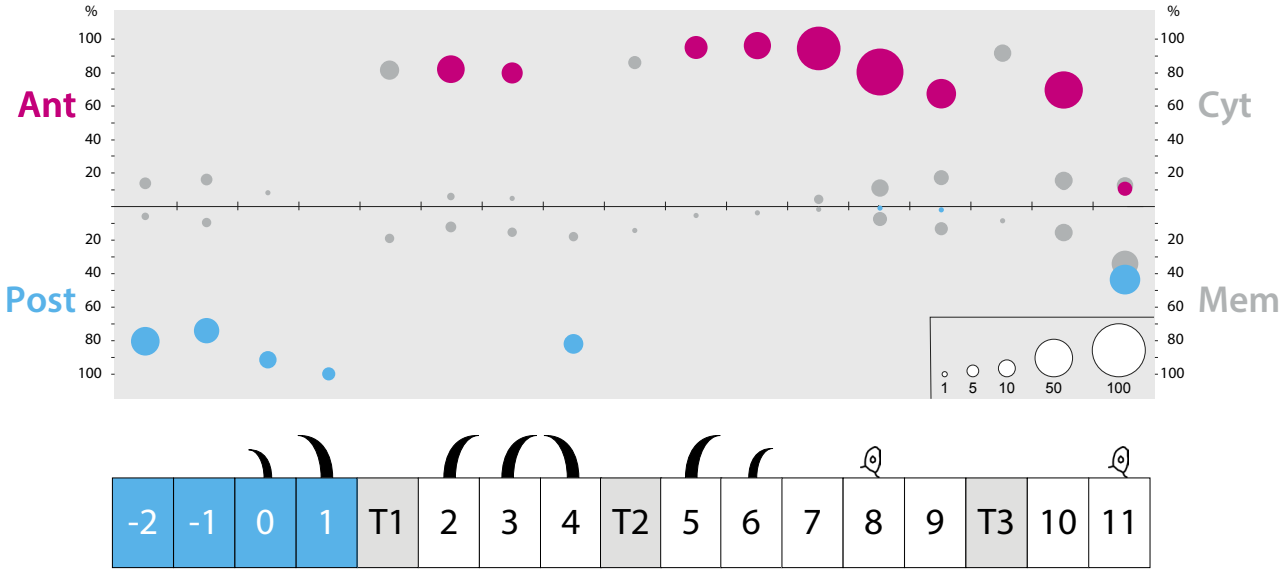

Pietra et al. Figure 6

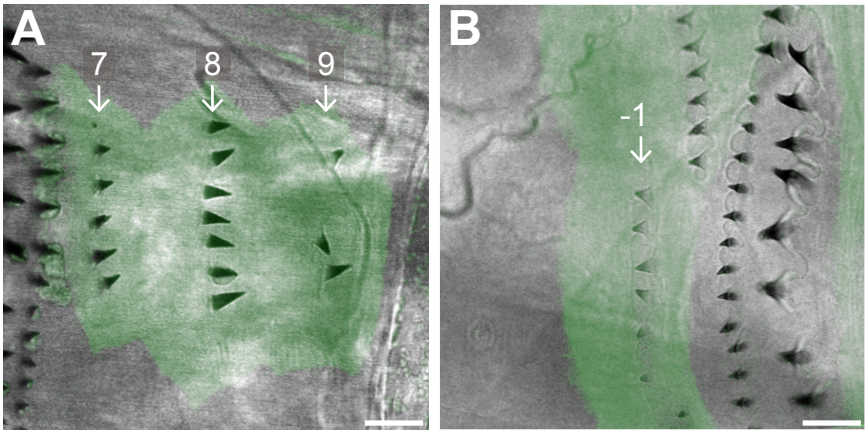

Pietra et al. Figure 7

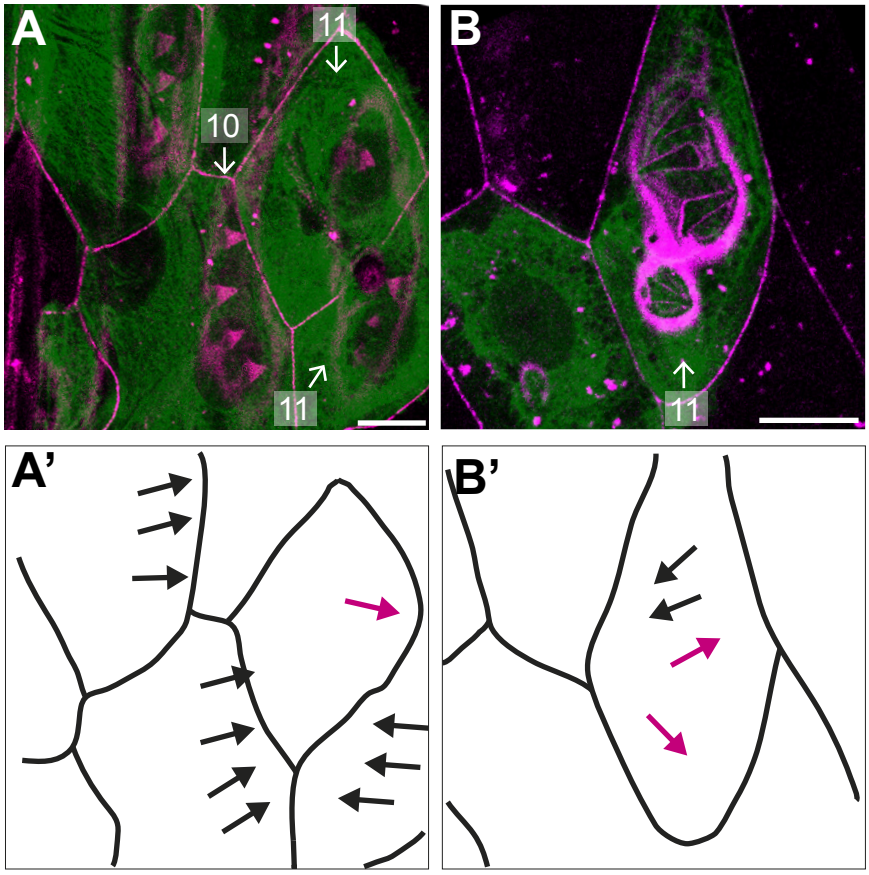

Pietra et al. Figure 7–figure supplement 1

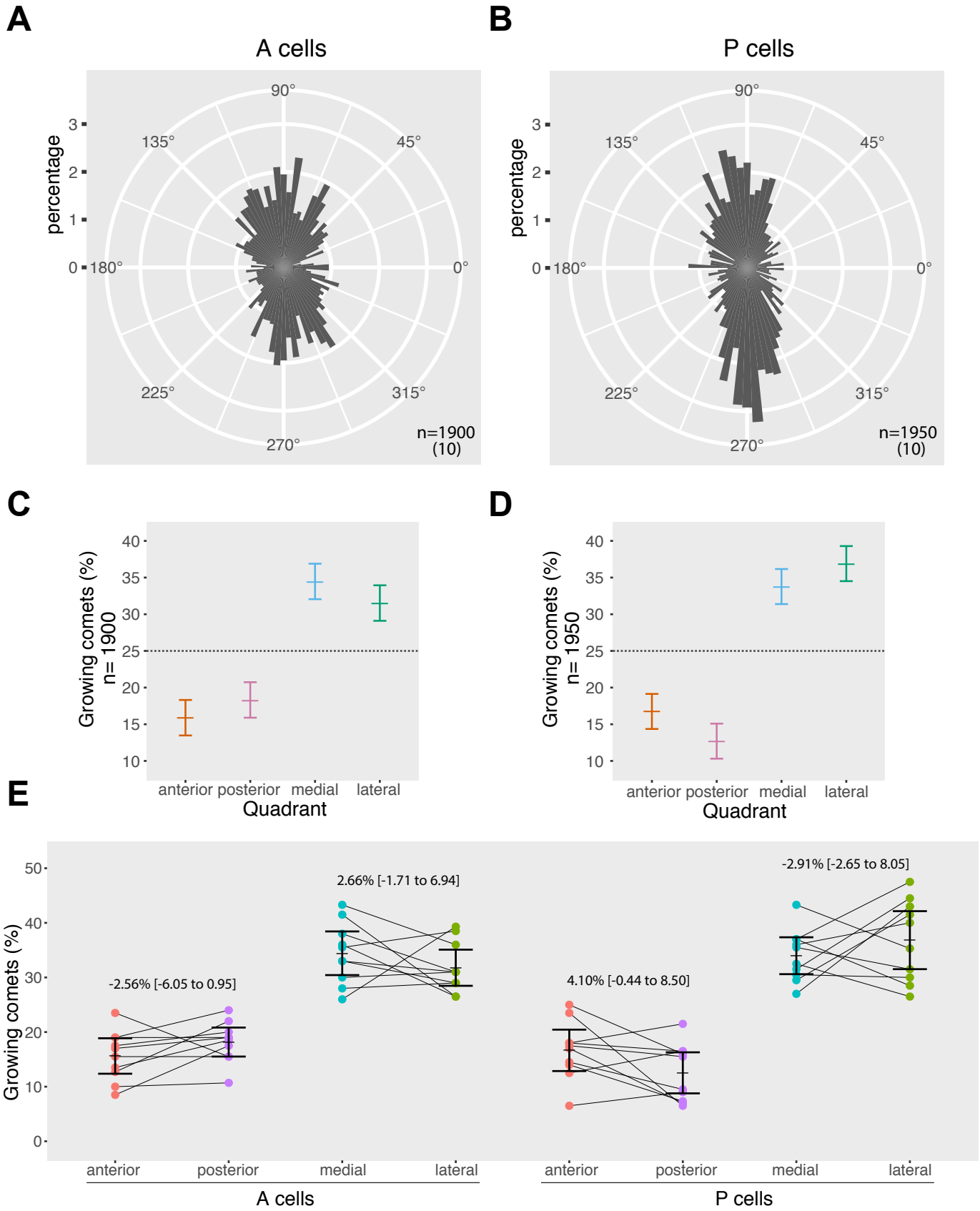

Pietra et al. Figure 8

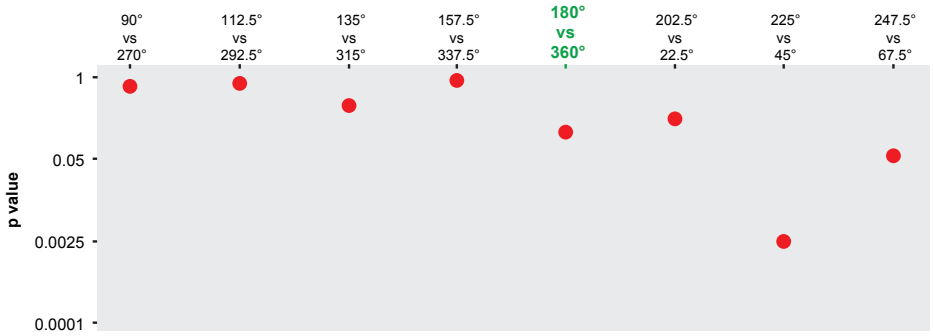

A larval cells

Sectors	Number of comets		p value
90° vs 270°	195	188	0.72
112.5° vs 292.5°	175	170	0.79
135° vs 315°	110	124	0.36
157.5° vs 337.5°	99	97	0.89
180° vs 360°	**56**	**73**	**0.13**
202.5° vs 22.5°	73	59	0.22
225° vs 45°	79	122	0.002
247.5° vs 67.5°	124	156	0.06

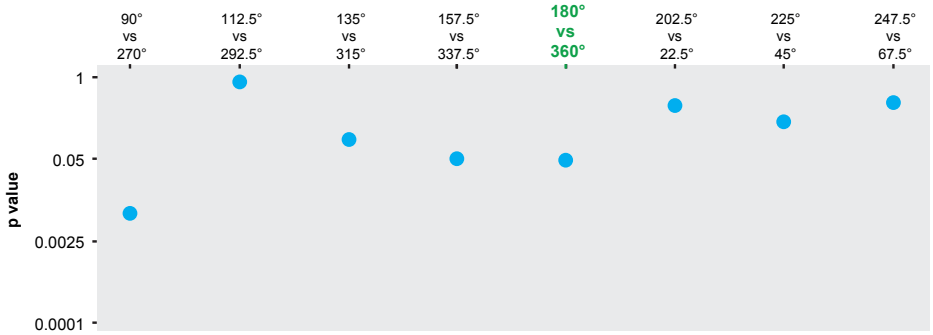

P larval cells

Sectors	Number of comets		p value
90° vs 270°	215	275	0.007
112.5° vs 292.5°	189	185	0.84
135° vs 315°	121	97	0.10
157.5° vs 337.5°	74	52	0.05
180° vs 360°	**86**	**62**	**0.05**
202.5° vs 22.5°	62	52	0.35
225° vs 45°	96	79	0.20
247.5° vs 67.5°	160	145	0.39

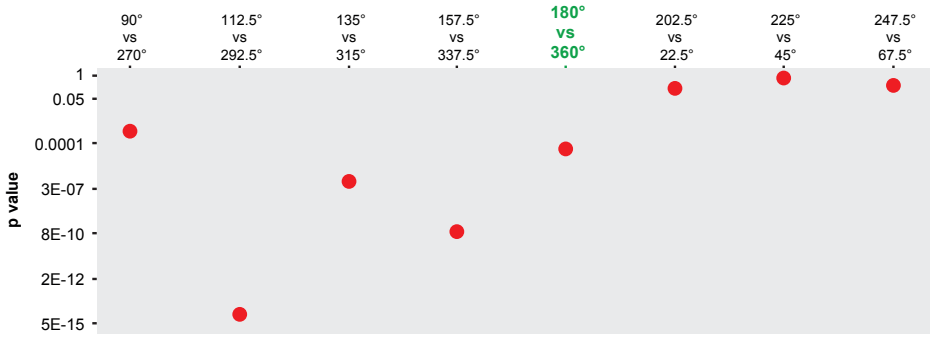

A pupal cells

Sectors	Number of comets		p value
90° vs 270°	658	789	0.0006
112.5° vs 292.5°	303	524	1.53E-14
135° vs 315°	180	287	7.37E-07
157.5° vs 337.5°	123	239	1.08E-09
180° vs 360°	**143**	**220**	**0.00005**
202.5° vs 22.5°	208	235	0.20
225° vs 45°	271	279	0.73
247.5° vs 67.5°	396	427	0.28

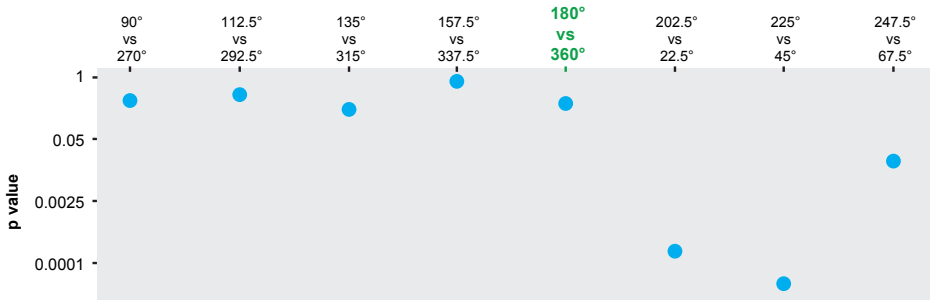

P pupal cells

Sectors	Number of comets		p value
90° vs 270°	299	323	0.34
112.5° vs 292.5°	117	129	0.44
135° vs 315°	55	69	0.21
157.5° vs 337.5°	56	54	0.85
180° vs 360°	**67**	**55**	**0.28**
202.5° vs 22.5°	86	44	0.0002
225° vs 45°	119	64	0.00005
247.5° vs 67.5°	155	116	0.02

Pietra et al. Figure 8–figure supplement 1

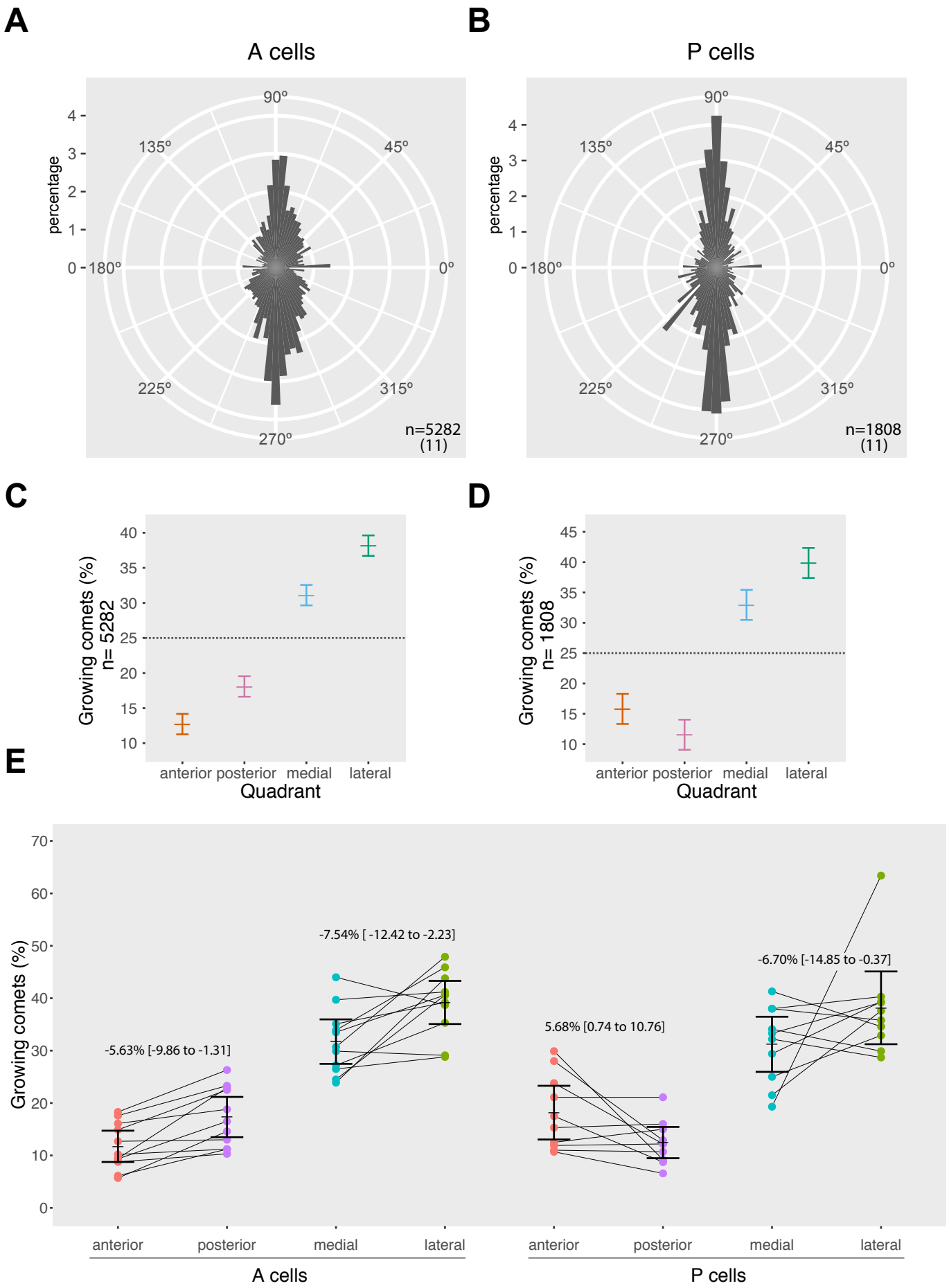

Pietra et al. Figure 8–figure supplement 2

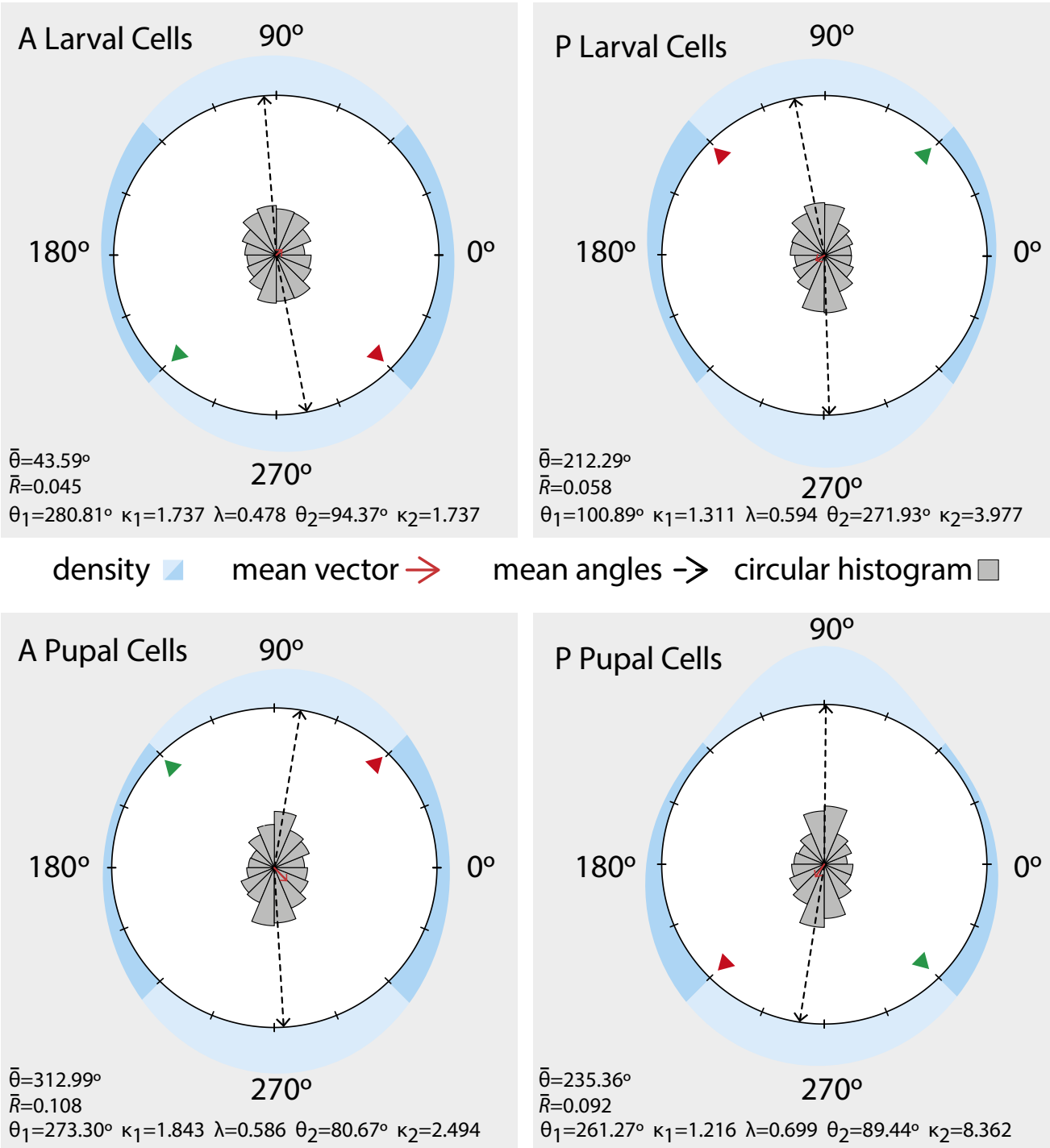

Pietra et al. Figure 8–figure supplement 3

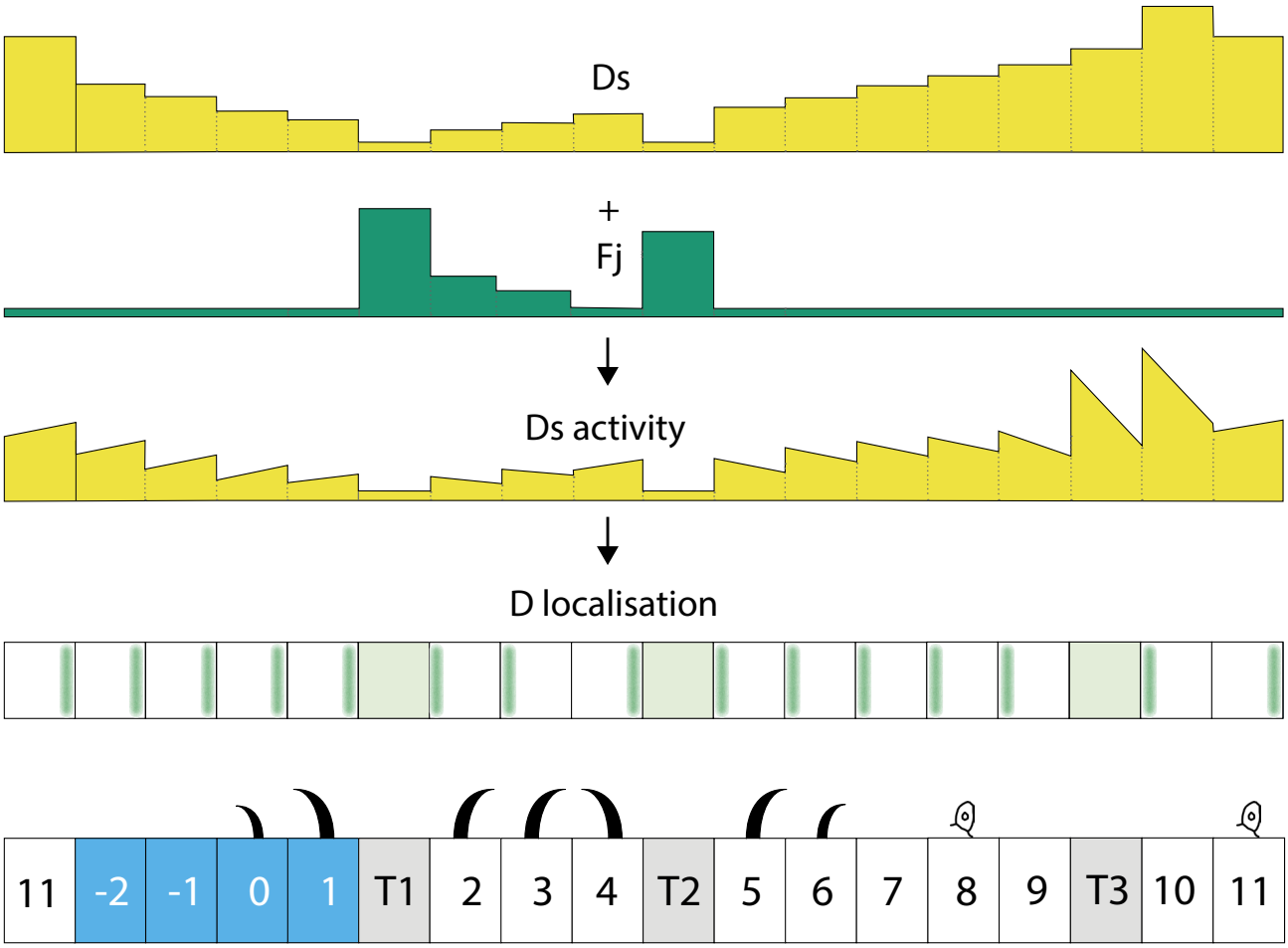

Pietra et al. Figure 9